Montana State University

Task Report No 3

A Feasibility Study of Road Culvert / Bridge Deck Deicing Using Geothermal Energy

By:

Ethan Turner (Graduate Student)

Mohammad Khosravi, Assistant Professor

Kathryn Plymesser, Assistant Professor

Kirsten Matteson, Assistant Professor

Ladean McKittrick, Assistant Teaching Professor

Prepared for:

Montana Department of Transportation

May 2023

TABLE OF CONTENTS

LIST OF FIGURES

LIST OF TABLES

STANDARD CONVERSION TABLE – ENGLISH TO METRIC				
Symbol	To convert from	Multiply by	To determine	Symbol
		LENGTH		
IN	inch	25.4	millimeters	mm
FT	feet	0.3048	meters	m
YD	yards	0.9144	meters	m
MI	miles	1.609344	kilometers	km
		AREA		
SI	square inches	645.16	square millimeters	mm^2
SF	square feet	0.09290304	square meters	m^2
SY	square yards	0.83612736	square meters	m^2
A	acres	0.4046856	hectares	ha
MI^2	square miles	2.59	square kilometers	km^2
		VOLUME		
CI	cubic inches	16.387064	cubic centimeters	cm^3
CF	cubic feet	0.0283168	cubic meters	m^3
CY	cubic yards	0.764555	cubic meters	m^3
GAL	gallons	3.78541	liters	L
OZ	fluid ounces	0.0295735	liters	L
MBM	thousand feet board	2.35974	cubic meters	m^3
		MASS		
LB	pounds	0.4535924	kilograms	kg
TON	short tons (2000 lbs)	0.9071848	metric tons	t
		PRESSURE AND STRESS		
PSF	pounds per square foot	47.8803	pascals	Pa
PSI	pounds per square inch	6.89476	kilopascals	kPa
PSI	pounds per square inch	0.00689476	megapascals	Mpa
		DISCHARGE		
CFS	cubic feet per second	0.02831	cubic meters per second	$m^3/_s$
		VELOCITY		
FT/SEC	feet per second	0.3048	meters per second	m/s
		INTENSITY		
IN/HR	inch per hour	25.4	millimeters per hour	mm/hr
		FORCE		
LB	pound (force)	4.448222	newtons	N
		POWER		
HP	horsepower	746.0	watts	W
		TEMPERATURE		
°F	degrees Fahrenheit	5 X (°F – 32)/9	degrees Celsius	°C
		DENSITY		
lb/ft^3	pounds per cubic foot	16.01846	kilograms per cubic meter	kg/m^3
		ACCELERATION		
g	freefall, standard	9.807	meters per second squared	m/s^2

TO CONVERT FROM METRIC TO ENGLISH, DIVIDE BY THE ABOVE CONVERSION FACTORS.

LIST OF PARAMETERS

C	Cementitious material content
CF	Coarseness factor
C_p	Heat capacity at constant pressure
h	Convective heat transfer coefficient
k	Thermal conductivity coefficient
N	Normal vector on the boundary
q	Conductive heat flux vector
Q	cumulative percent retained on a 3/8" sieve
R	cumulative percent retained on the No. 8 sieve
T	Absolute temperature
T_{ext}	External temperature
T_s	Surface temperature
W	percent passing the No. 8 sieve
WF	Workability factor
ε	Surface emissivity
ρ	Density
σ	Stefan-Boltzmann constant
∇T	Temperature gradient

CHAPTER 1: INTRODUCTION

Weather conditions during Montana winters pose two challenges for concrete bridges: 1) the removal of accumulated snow and ice and 2) deterioration due to temperature fluctuations. While there are current methods for snow and ice removal, there is potential for improvement with regards to cost, effectiveness, and environmental impacts. Deterioration is an issue because when the temperature falls below 0 °C, the water in the concrete expands which can cause damage through cracking. As the concrete in bridge decks cracks and spalls, the steel reinforcement is exposed which leads to corrosion and further deterioration of the bridge deck. A ground-source bridge deck deicing system can mitigate temperature fluctuations within concrete bridge decks, and thus reduce the effects of concrete deterioration. It can also be a means of effective removal of accumulated snow and ice. Ground-source bridge deck deicing systems extract heat from the earth and transfer it into the concrete through a closed loop system of heat exchanger pipes embedded in the ground and the concrete bridge deck. Heat transferred from the earth to the concrete reduces temperature fluctuations in the bridge deck.

A survey was conducted among Montana Department of Transportation (MDT) staff to understand their perceptions and preferences concerning snow and ice removal and prevention methods in Montana. Results from the survey show that the three most used methods by MDT are: 1) anti-icing to prevent snow or ice accumulation on the surface before a winter storm, 2) deicing to remove snow and ice during and after a storm, and 3) mechanical removal. The effectiveness of each method in clearing roads and enhancing traction depends on various factors including weather conditions, pavement temperature, snow thickness, and ice accumulation. Anti-icing methods are typically employed before a winter weather event or in the initial stages of a storm, while deicing methods are used during and after winter weather events when the road surface is covered with a significant amount of snow. Mechanical removal methods are used alone or in combination with other methods during or after a winter weather event. While not used to remove or prevent snow and ice, applying abrasives to road surfaces can play an important role during low-temperature events by increasing traction.

The survey results indicate that the selection of deicing and anti-icing methods and materials depends on various factors, including their effectiveness, cost, environmental impact, ease of application, availability, public feedback, and impact on corrosion. In Montana, the most used materials for deicing or anti-icing bridge decks are salts and other debonding chemicals such as Sodium Chloride (NaCl), Magnesium Chloride (MgCl2), and Potassium Acetate (KAc). However, studies have shown that deicing chemicals have negative environmental impacts (e.g., Kelting & Laxon, 2010; Shi et al., 2018) and can accelerate the corrosion of steel reinforcement, leading to the collapse of reinforced concrete bridge decks (e.g., Baboian, 1992; Granata & Hartt, 2009; Virmani et al., 1983; Virmani et al., 1984; White et al., 2005; Yunovich et al., 2003). Abrasives, such as crushed stone from local gravel sources, are also frequently used for bridge decks in Montana. However, studies indicate that they can contribute to environmental problems, such as water and air quality, and increase maintenance costs, including road and shoulder clean-up after the winter season (Fischel, 2001).

This task report contains the construction procedure of a physical bridge deck model used to investigate the feasibility of using geothermal energy for bridge deck deicing in Montana. The

bridge deck model is being tested in the Cold Hydrodynamics Chamber (CHC) in Montana State University's Subzero Research Laboratory (SRL) to further calibrate and refine an existing numerical model. This report starts with a presentation of the final concrete mix design for the bridge deck model (Chapter 2). Chapter 3 describes the creation and validation of a numerical simulation of a geothermal bridge deck. It also describes the simulations used to evaluate the significance of various parameters in the design of a physical bridge deck model. The chapter concludes with the final design of a physical bridge deck model. Chapter 4 details the construction of the physical bridge deck model and instrumentation. Chapter 5 includes a discussion of Montana weather with data from Road Weather Information System (RWIS) stations, as well as the results of a survey distributed to the MDT. Chapter 6 summarizes preliminary test results of a physical bridge deck model experiment.

CHAPTER 2: CONCRETE MIX DESIGN TESTS

The concrete mix design in Task Report 2 (Pourakbar et al., 2021) was developed from a series of tests to determine the cement, aggregate, and water requirements and proportions. No admixtures were chosen for the final mix design.

Cement

Type I/II Portland Cement from Grupo Cementos de Chihuahua's (GCC's) Trident Plant was chosen for this mix design. Type I/II Portland Cement is a general-purpose cement widely used in bridges, foundations, walls, driveways, sidewalks, etc.

Concrete Aggregate Combined Gradation

The coarse and fine aggregates were obtained from Bozeman Brick Block and Tile. Three optimization charts were used to validate the aggregates: 1) the Coarseness Factor chart, 2) the 0.45 Power chart, and 3) the Percent Retained chart. Each chart represents one aspect of an optimized aggregate gradation. The coarseness factor chart, also known as the Shilstone Chart, is a method for determining if the combined aggregate gradation is considered optimized. The chart helps describe the relationship between coarseness factor and workability factor of a concrete mix. The coarseness factor (x-axis) and workability factor (y-axis), both represented in percentages, can be calculated using Equations (1) and (2), respectively:

$$CF\ (\%) = \frac{Q}{R} \times 100 \tag{1}$$

$$WF\ (\%) = W + \frac{2.5 \times (C - 564)}{94} \tag{2}$$

where Q is the cumulative % retained on a 3/8" sieve, R is the cumulative % retained on the No. 8 sieve, W is the percent passing the No. 8 sieve, and C is the cementitious material content in lb/yd³. Figure 1 shows the grain size distribution curves for the aggregates obtained from Bozeman Brick Block and Tile.

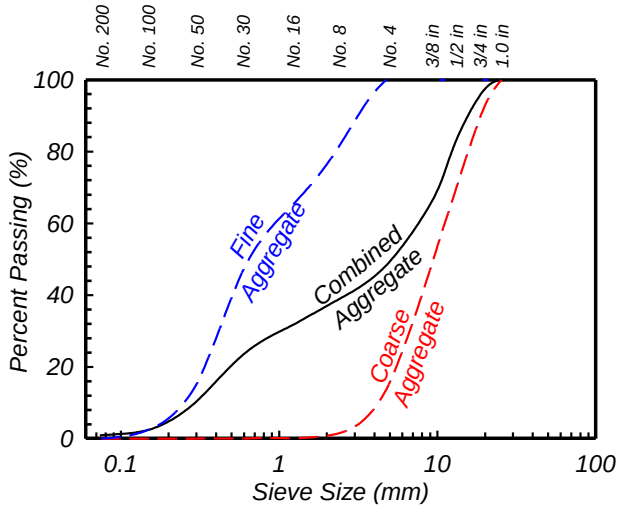

Figure 1. Individual grain size distribution curves

Figure 2 illustrates the coarseness factor chart for the proposed concrete mix design. The chart is divided into four zones, with Zone II generally considered as the most suitable for creating a concrete mix with reasonable workability and durability. Aggregates that plot near the boundaries of or outside Zone II are more likely to cause problems during concrete placement or lead to reduced overall durability of the hardened concrete. As shown in Figure 2, the combined aggregates used in the proposed mix design fall squarely within Zone II, as desired.

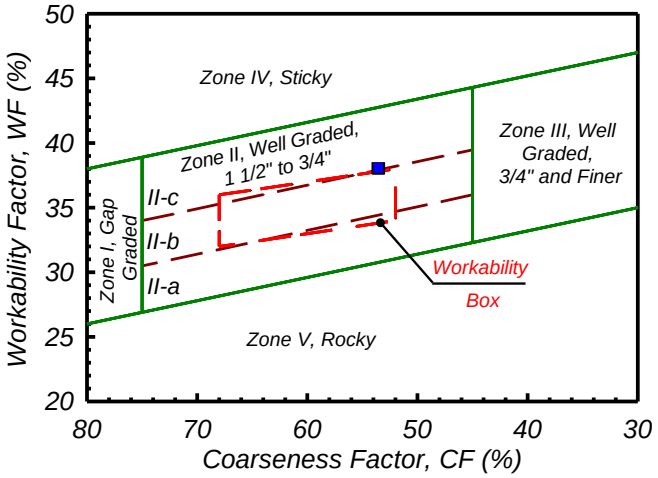

Figure 2. Coarseness Factor chart of concrete mix designs

The 0.45 power line is a method used to predict voids in the concrete's combined aggregates. Figure 3(a) shows the 0.45 power line which is developed based on the nominal maximum size of the combined aggregates. A gradation line that passes above the power line represents fine aggregates, while the one below the line represents coarse aggregates. Figure 3(a) shows the grain size distribution of the combined aggregates and the power line. The grading curves for the portion of the combined aggregate passing the No. 30 sieve mostly falls below the power chart line leaving room for the cementitious materials in the final mix. Figure 3(a) demonstrates that the combined grading is within ± 7 percentage points of the Power Chart line.

The individual percent retained chart (i.e., Haystack Plot) is a method to describe the excess or lacking combined aggregate sizes in the mixture. The chart can also be used to identify workable mixes with a reasonably low water demand. Plots are restricted with high and low lines, generally between 18-22% and 5-12%, respectively. To prevent segregation, it is generally recommended to have at least a total of 13% of the combined aggregate retained on any two adjacent sieves. Figure 3(b) demonstrates the percent retained on each sieve (y-axis) of the concrete mix design for each sieve size. In this case, the upper limit is 20% and the lower limit is 8%. As shown here, the concrete mix falls between the "High" and "Low" line, suggesting that the mix is workable and has a reasonably low water demand.

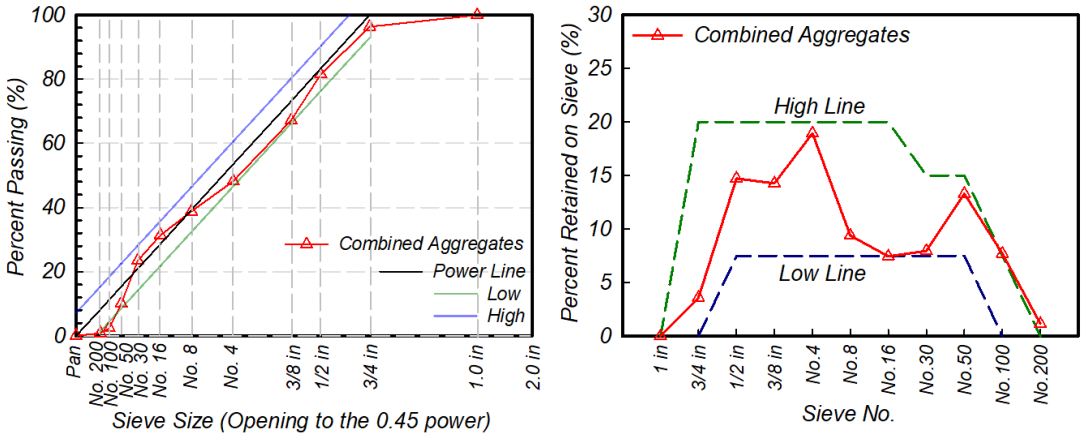

(a) *(b)*

Figure 3. a) 0.45 Power Chart, and b) Percent Retained Chart of the collected mix designs

Final Mix Design

A series of tests were conducted to verify the final mix design reported in Task Report 2 (Pourakbar et al., 2021). These tests revealed that the mix design needed more water for adequate workability. Compressive strength tests were conducted in accordance with ASTM C39 to assure 7-day strength requirements were met despite the added water. Table 1 shows the final mix design for a 1.5 ft^3 mix.

Table 1. Mix proportions for 1.5 ft^3 mix

Item	***Item Type***	***Amount (lbs)***
Water	-	19.88
Portland Cement	Type I/II from Trident GCC	31.74
Fine Aggregate	O.D. BBB&T Concrete Sand	66.72
Coarse Aggregate		83.52

CHAPTER 3: BRIDGE DECK MODEL DESIGN

Data from experiments conducted by Bowers Jr (2016) at Virginia Tech Geotechnical Research Facility was used to create and validate a numerical simulation in COMSOL Multiphysics. Once validated, parametric studies were conducted within the simulation to determine the most significant parameters in the design of a geothermal bridge deck model.

Overview of Past Field Test

The thermal performance of a small-scale bridge deck deicing system was investigated by Bowers Jr (2016). Two bridge deck models were constructed at 1.3 m wide, 3.05 m long, and 0.254 m deep. Cross-linked polyethylene (PEX) tubing with an inner diameter of 16 mm and a thickness of 3 mm (OD 22 mm) was used for heat exchanger pipes. The spacings of the pipes for the two models were 20.3 cm and 30.5 cm. A 20% glycol solution with a flow rate of 15.1 L/m was used as the circulating fluid. The temperature at various locations throughout both models was measured using several imbedded thermistors. Figure 4(b) shows the cross-sectional locations of the thermistors at one location in the model. Virginia Department of Transportation class A4 concrete mixture, which has a minimum 28-day compressive strength of 27.6 MPa, was used in the bridge deck models. Among the various weather conditions tested by Bowers Jr (2016), a severe winter weather event that occurred on February 20-22, 2015, in Blacksburg, VA, was explored. Figure 4(a) shows the conditions during the winter weather event.

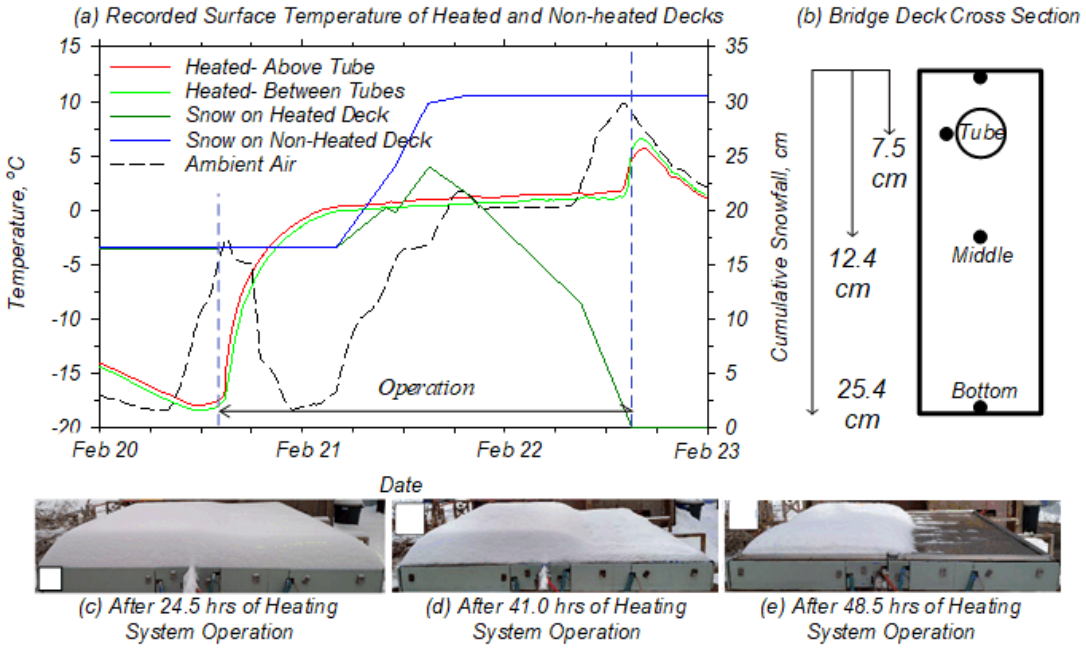

Figure 4. a) Recorded surface temperature of the heated and non-heated decks, ambient temperature, cumulative snowfall; b) cross-sectional location of studied thermistors; and photo of the deck model surface during the storm after: c) 24.5 hours, d) 41 hours, and e) 48.5 hours (Bowers Jr, 2016).

A snowstorm occurred before the winter weather event that deposited 20 cm of snow. The bridge deck with the heat exchanger pipe spacing of 20.5 cm began heating after the snowstorm at 14:30 on February 20, 2015. The other bridge deck was not heated and served as a control for the experiment. When the heating was initiated, the temperature and snow depth for both deck surfaces was -18 °C and 16.5 cm, respectively. At 23:30 on February 20, 2015 (9 hours of heating), the

average temperature of the surface of the heated bridge deck was above the freezing point despite a 15 °C drop in ambient temperature. The temperature of the surface of the heated bridge deck remained above freezing throughout the rest of the winter weather event. Figure 4(c) shows the bridge decks at 15:00 on February 21, 2015 (24.5 hours of heating). The snow depth on the non-heated and heated bridge decks was 29.8 cm and 24.1 cm, respectively. Figure 4(d) shows the bridge decks at 7:30 on February 22, 2015 (41 hours of heating). The snow depth of the heated bridge deck dropped to 11.4 cm. Figure 4(e) shows the bridge decks at 15:00 on February 22, 2015 (48.5 hours of heating). By this time, the heated bridge deck was free from snow while the non-heated bridge deck still had a snow depth of 30.5 cm.

Overview of Numerical Simulation

Modeling the bridge deck deicing process is complicated due to the involvement of different heat transfer mechanisms and unsteady weather conditions. The model of a ground-source bridge deck deicing system involves multiple heat transfer mechanisms including conduction, convection, radiation (solar and thermal), and snow melting heat flux. This section presents the results of a 3D numerical model developed to assess the performance of a bridge deck deicing system. The results from the bridge deck heating experiments conducted by Bowers Jr (2016) were first used to validate the numerical model. The validated numerical model was then used to evaluate the performance and feasibility of bridge deck deicing using geothermal energy for Montana weather conditions.

Numerical Model Validation Using Data from Bowers Jr (2016)

A 3D numerical model was constructed using the finite element software COMSOL Multiphysics. The heat transfer mechanisms were expressed within the software as follows:

Conduction occurs between the circulating fluid and pipe walls and between the pipe and surrounding concrete. For completely insulated boundary conditions (e.g., insulation effect of snow accumulation on the surface), the heat flux, $q = -k\nabla T$, at a surface is equal to zero due to a Neumann boundary condition. Equation (3) presents the heat conduction in the slab in a Neumann boundary condition.

$$\rho C_p \frac{\partial T}{\partial t} + \nabla \cdot (-k\nabla T) = 0 \tag{3}$$

where ρ is the density (kg/m^3), C_p is the heat capacity at constant pressure (J/(kg·K)), T is the absolute temperature (K), $\partial T/\partial t$ is a time derivatives operator, k is the thermal conductivity coefficient (W/m·K), and ∇T is the temperature gradient.

The bottom and top surfaces (when not insulated by snow) are exposed to the environment, and thus will experience both convection and radiation. Convection is expressed in Equation (4):

$$-n.\, q = \mathrm{h} \cdot (T_{ext} - T_s) \tag{4}$$

where n is the normal vector on the boundary, h is the convective heat transfer coefficient (W/m^2 ·K), T_{ext} is the external temperature, and T_s is the surface temperature (K). Radiation is expressed in Equation (5):

$$-n.\, q = \varepsilon\sigma(T_{ext}^4 - T_s^4) \tag{5}$$

where ε is the surface emissivity and σ is the Stefan-Boltzmann constant (a predefined physical constant, 5.67×10^{-8} $(W\cdot m^2)/K^4$). The snow melting process was not considered in these analyses.

The dimensions and material properties were chosen to replicate the field tests by Bowers Jr (2016) for validation purposes. Figure 5(a) and (b) show an isometric view of the model and the meshed model. The model includes the circulating fluid, the heat exchanger pipes, and the concrete deck. 1D linear elements were used for the fluid flow and heat transfer in the heat exchanger pipes. The flow rate, pressure, and temperature were modeled as the average cross-section quantities, so they only vary along the length of the pipes. Friction factors were used to account for head loss in the pipes. External wall resistance was added to account for the thickness and thermal conductivity of the pipe wall. The steel reinforcement was not included in the model, but rather, to account for the effects of the rebar, the model was split into three zones through the depth. The material properties for each zone were based on a volumetric average of the concrete and steel reinforcement in each zone. The top and bottom zones have steel reinforcement, while the middle zone does not have steel reinforcement.

To validate the model, the severe winter weather event (February 20-22, 2015) described previously was replicated. Figure 5(c) shows the COMSOL predicted vs. Bowers Jr (2016) measured temperature at various locations at a cross-section with a heat exchanger pipe. Figure 5(d) shows the cross-sectional and top surface temperature of the bridge deck after 12 hours of heating. The numerical model accurately predicted the temperature within the Bowers Jr (2016) bridge deck model.

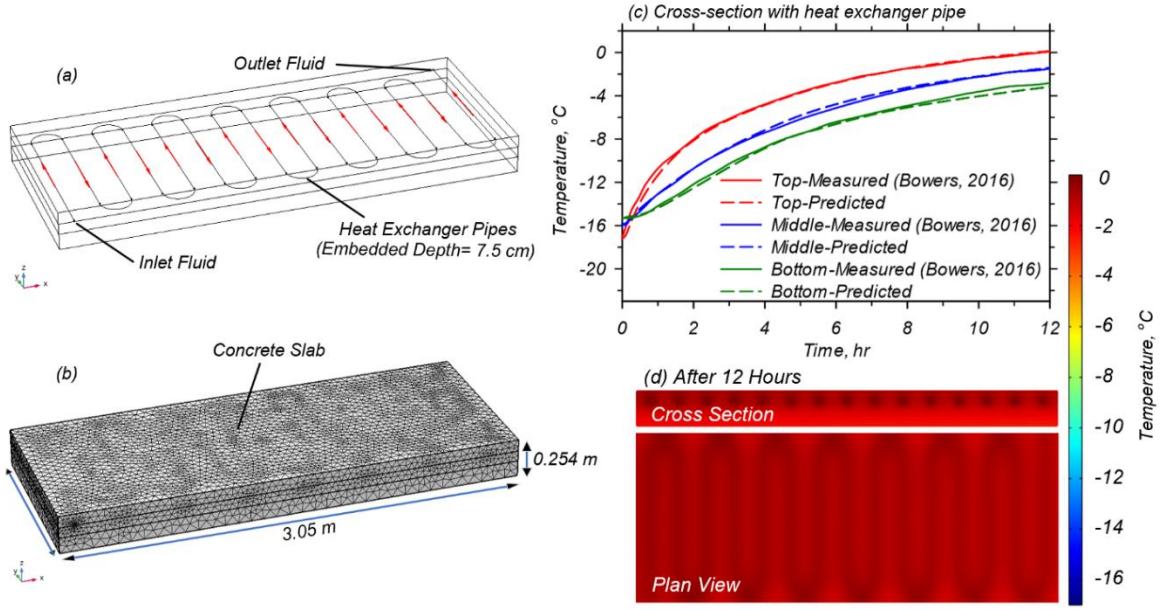

Figure 5. a) Bridge deck model configuration, b) meshed 3D model, c) comparison between experimental results and numerically predicted values of temperature at the top, middle, and bottom of the bridge deck at cross-section with heat exchanger pipes, and d) cross-sectional and top surface temperature of the bridge deck after 12 hours of heating.

Parametric Study

A parametric study was developed to evaluate the influence of the ambient temperature, deck dimensions, top reinforcement cover, inlet flow rate, heat exchanger tube spacing, and inlet fluid

temperature on the ability of a geothermal bridge deck deicing system to raise the top surface temperature above 0 °C. The results from these studies were used in the design of the bridge deck model.

Ambient Temperature

The effect of ambient temperature on top surface temperature of a geothermally heated bridge deck was tested to evaluate the importance of the parameter in the operation and design of the bridge deck model. Besides ambient temperature, all other testing variables were constant between tests. The inlet fluid temperature was 6 °C. Nine different ambient temperatures were tested, with the highest being -0.5 °C and the lowest being -17 °C. The top surface temperature of the test with ambient temperature of -0.5 °C took around 0.6 hours to reach 0 °C. The top surface temperature of the test with ambient temperature of -17 °C took around 9.2 hours to reach 0 °C. Figure 6 shows the top surface temperatures from these tests along with top surface temperatures for tests with the intermediate ambient temperatures. As expected, the results suggest that as the ambient temperature increases, the time it takes for the geothermal system to raise the top surface temperature above 0 °C decreases.

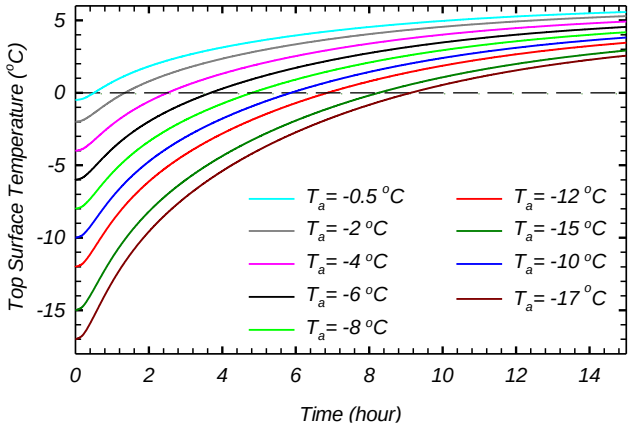

Figure 6. Parametric study results for ambient temperature

Bridge Deck Dimensions

A parametric study for bridge deck dimensions was conducted because the base model, which measures 3.05 m long, 1.30 m wide, and 0.25 m deep, is too large to be tested in the CHC. A smaller model was developed to determine whether it could produce similar results to the base model in the ambient temperature study. The smaller model had dimensions of 1.50 m long, 1.20 m wide, and 0.20 m deep. Figure 7(b) shows a schematic of both models. The smaller model was tested with ambient temperatures of -4 °C and -12 °C. At an ambient temperature of -4 °C the top surface temperature of the smaller model took 2.8 hours to reach 0 °C, while the base model took 2.6 hours. At an ambient temperature of -12 °C the top surface temperature of the smaller model took 7.5 hours to reach 0 °C, while the base model took 6.9 hours. Figure 7(a) shows the top surface temperature of both the base model and smaller model at ambient temperatures of -4 °C and -12 °C. The results suggest that there is a negligible difference in the ability of the base model and a smaller model to bring the top surface temperature to 0 °C.

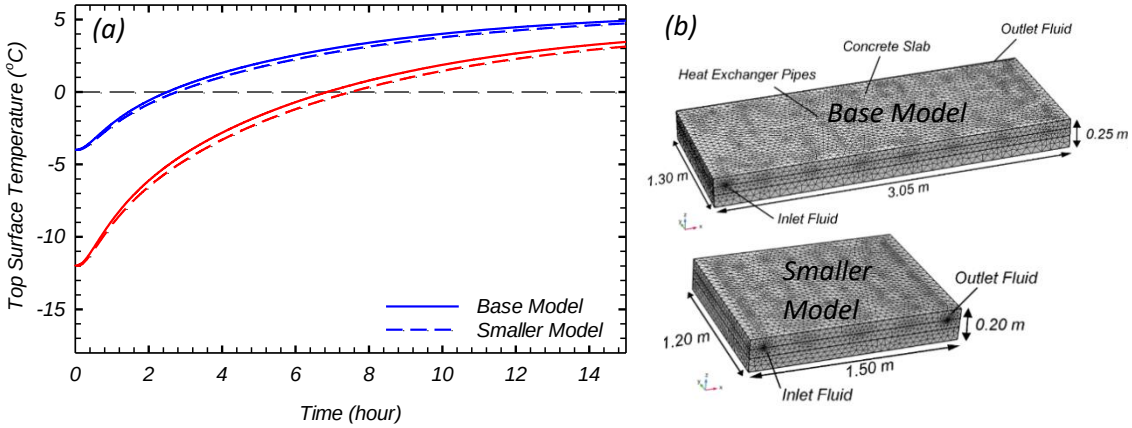

Figure 7. a) Parametric study results for Base Model and Smaller Model and b) schematic of Base Model and Smaller Model

Top Reinforcement Cover

In a physical bridge deck model, the heat exchanger tubes are typically attached to the bottom of the top reinforcement. The effect of top reinforcement cover was tested to evaluate the importance of the depth of the heat exchanger tubes in the design of a geothermal bridge deck. The top surface temperature was found for models with top reinforcement covers of 4.5 cm, 5.5 cm, and 6.0 cm. All other parameters were constant for the three tests. The ambient temperature and inlet fluid temperature were -17 °C and 6 °C, respectively. The top surface temperature of the 4.5 cm, 5.5 cm, and 6.0 cm cover tests took 8.2 hours, 8.5 hours, and 8.8 hours to reach 0 °C, respectively. Figure 8(a) shows the top surface temperature for each top reinforcement cover condition. As expected, the results suggest that as top reinforcement cover decreases, the time it takes for the geothermal system to raise the top surface temperature above 0 °C also decreases. The difference, however, between top reinforcement cover conditions between 4.5 cm and 6.0 cm is negligible.

Inlet Fluid Flow Rate

The effect of inlet fluid flow rate was tested because the calibrated numerical model uses a flow rate greater than the maximum flow rate in the CHC. The top surface temperature was evaluated for the 15 L/min flow rate used by Bowers Jr (2016), as well as flow rates of 10 L/min, 15 L/min, 20 L/min, and 25 L/min. All other parameters were constant for the four tests. The ambient temperature and inlet fluid temperature were -17 °C and 6 °C, respectively. The top surface temperature of the 10 L/min, 15 L/min, 20 L/min, and 25 L/min flow rate tests took 8.9 hours, 8.2 hours, 8 hours, and 7.9 hours to reach 0 °C, respectively. Figure 8(b) shows the top surface temperature for each inlet fluid flow rate condition. The results suggest that as the flow rate increases, the time it takes for the geothermal system to raise the top surface temperature above 0 °C decreases. The difference, however, between inlet fluid flow rate conditions between 10 L/min and 25 L/min is negligible.

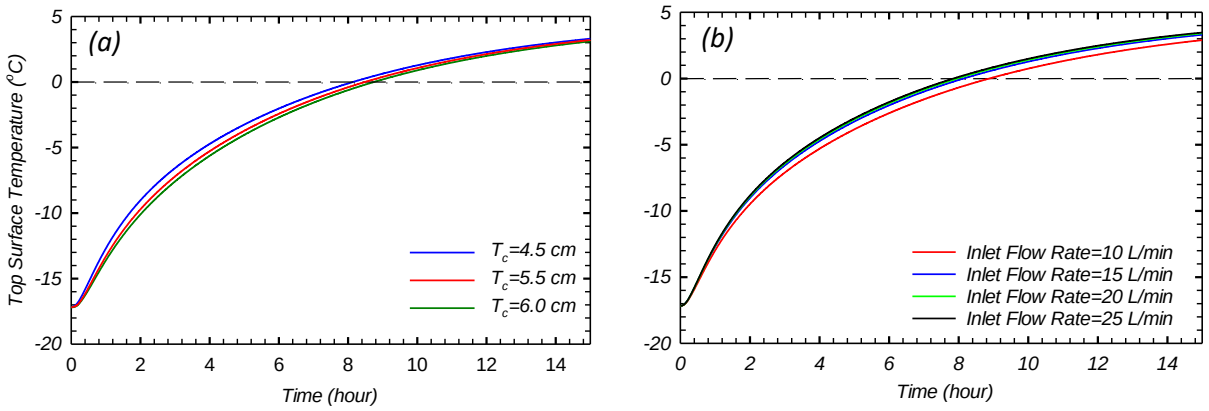

Figure 8. Parametric study results for a) top reinforcement cover and b) inlet fluid flow rate

Heat Exchanger Tube Spacing

The effect of heat exchanger tube spacing was tested to evaluate the importance of the parameter in the operation of a geothermal bridge deck. The top surface temperature was modeled for heat exchanger tube spacings of 15 cm, 20 cm, and 30 cm. All other parameters were constant for the three tests. The ambient temperature and inlet fluid temperature were set at -17 °C and 6 °C, respectively. The top surface temperature of the 15 cm, 20 cm, and 30 cm spacing tests took 5.5 hours, 8.2 hours, and 14.2 hours to reach 0 °C, respectively. Figure 9(a) shows the top surface temperature for each tube spacing condition. The results suggest that as heat exchanger tube spacing decreases, the time it takes for the geothermal system to raise the top surface temperature above 0 °C decreases.

Inlet Fluid Temperature

The effect of inlet fluid temperature was tested to evaluate the importance of the parameter in the operation of a geothermal bridge deck. Nine different inlet fluid temperatures were modeled, representing the range of mean earth temperatures in Montana, with the highest being 10.0 °C and the lowest being 6.0 °C. All other parameters were constant for the tests, with the ambient temperature set at -17 °C. The top surface temperature of the 10.0 °C and 6.0 °C inlet fluid temperature tests took 6.2 hours and 9.1 hours to reach 0 °C, respectively. Figure 9(b) shows the top surface temperature for each inlet fluid temperature condition. The results suggest that as inlet fluid temperature increases, the time it takes for the geothermal system to raise the top surface temperature above 0 °C decreases.

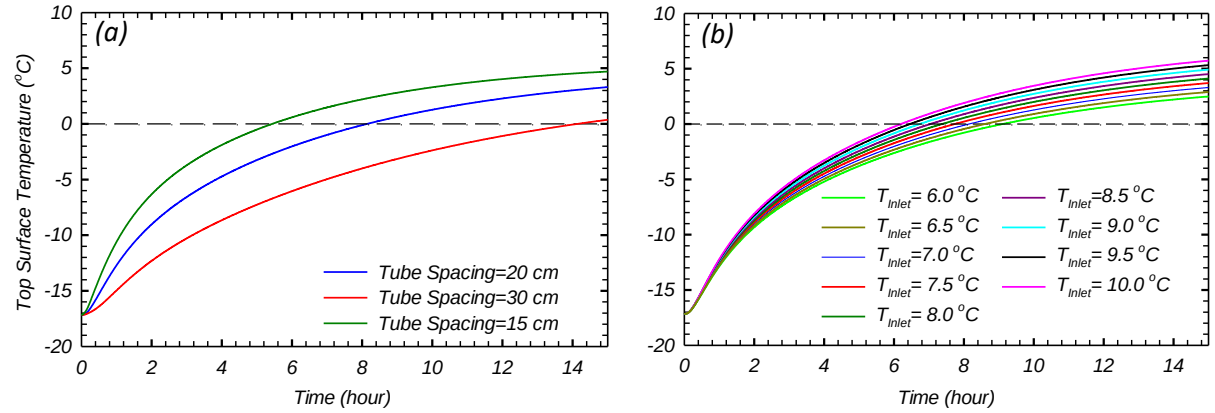

Figure 9. Parametric study of a) heat exchanger pipe spacing and b) inlet fluid temperature

Summary of Parametric Study

The effects of bridge deck dimensions, top reinforcement cover, and inlet fluid flow rate are negligible in the design of a geothermal bridge deck model. Any discrepancy in Montana code for reinforcement cover or the CHC's limitations for bridge deck dimensions and inlet fluid flow rate will not significantly affect the simulation's validation based on the past field tests. The effects of ambient temperature, heat exchanger tube spacing, and inlet fluid temperature are significant in the design of a geothermal bridge deck model. The heat exchanger tube spacing will match the design of the past field tests to assure validation of the simulation. The ambient and inlet fluid temperatures will be consistent with Montana's weather and geothermal conditions to accurately assess the feasibility of using geothermal energy to deice bridges in Montana.

Physical Model Design

While most of the experimental bridge deck design replicated Bowers Jr's bridge deck (2016), two model parameters were modified due to the limitations of the CHC. The bridge deck model was designed to be 1.0 m wide, 1.6 m long, and 0.2 m deep. The 1.0 m width allows the bridge deck model to fit through the CHC door. Figure 10 shows a schematic of the proposed bridge deck model. A flow rate of 5.5 L/min will be used because it is the maximum flow rate provided by the CHC. Other design parameters include 1.27 mm cross-linked polyethylene (PEX) tubing for the heat exchanger tubes with 20 cm spacing and a 30% propylene glycol solution for the circulating fluid. Refer to Appendix 1 for more detailed drawings of the model.

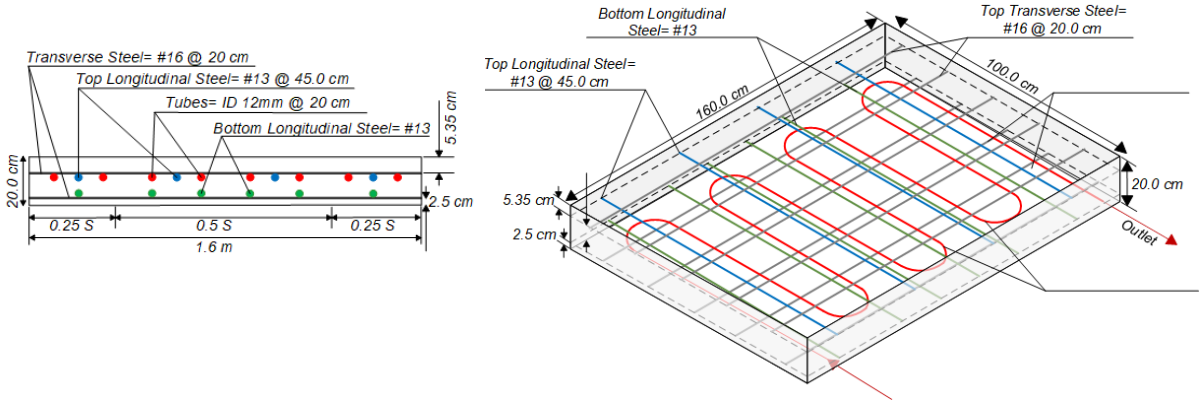

Figure 10. Proposed bridge deck model schematic

CHAPTER 4: MODEL CONSTRUCTION AND INSTRUMENTATION

In the spring and summer of 2022, the bridge deck model was constructed and prepared for testing. The required instrumentation was prepared and installed for data acquisition.

Form Construction

The bridge deck model was constructed in Montana State University's Bulk Materials Lab. To construct the formwork, Douglas-fir 2×10s and corrugated steel were utilized. The boundary conditions for this experiment require the top and bottom of the concrete to be uninsulated. Rather than removing the specimen from the form to expose the bottom, corrugated steel is the permanent bottom of the specimen. Because concrete's thermal conductivity is 1-3 W/mK, and steel's is much greater at approximately 50 W/mK, the steel bottom does not insulate the bottom of the concrete (Nagy & Szagri, 2018). Figure 11(a) shows the bridge deck model form. Once the formwork was constructed, steel reinforcement grids were configured according to the specifications with rebar ties. Figure 11(b) shows the finished steel reinforcement grids. PEX tubing was then attached to the top reinforcement grid using rebar ties.

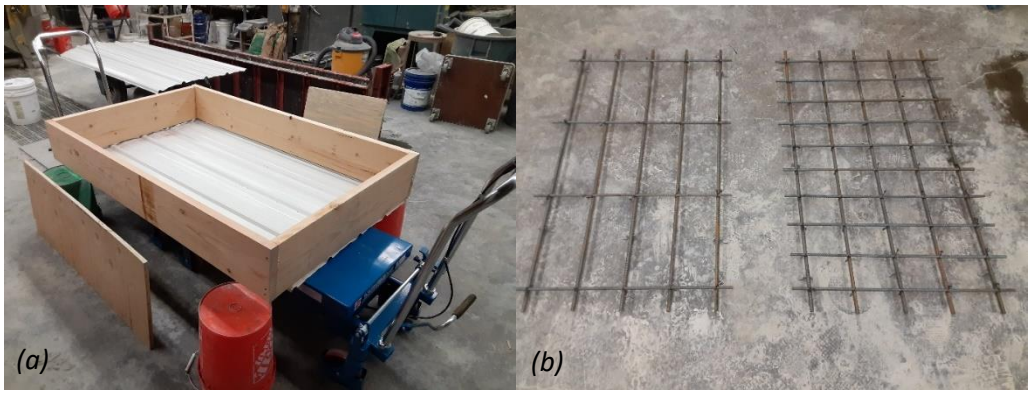

Figure 11. a) Bridge deck model form and b) finished reinforcement grids

The bottom reinforcement grid was then placed on plastic rebar chairs, facilitating the appropriate clear cover, while the top reinforcement grid was hung from additional steel set on the top of the forms with wire. To finish the form, two 12.7 mm holes were drilled in the form work to allow the PEX tubing to run through, and duct tape was used to mark the "fill line." Figure 12 shows the completed form without thermocouples. Thermocouple preparation and placement is discussed later in this chapter.

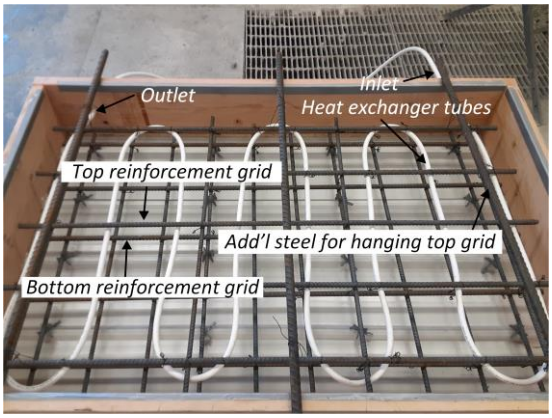

Figure 12. Completed form without thermocouples

Concrete Mixing, Pouring, and Curing

To facilitate later transport of the specimen, the formwork was placed on scissor lift carts and cinder blocks. Four batches of concrete were needed to reach the "fill line" and 32 compression cylinders were cast. Once the top surface was finished, the form was covered in plastic wrap for 24 hours. After 24 hours, the plastic wrap was replaced with wetted towels on the concrete surface and a plastic tarp to trap moisture. Figure 13(a) and (b) show this process. The towels were re-wetted every two days during the 28-day curing period. Curing took place in the laboratory, kept at room temperature.

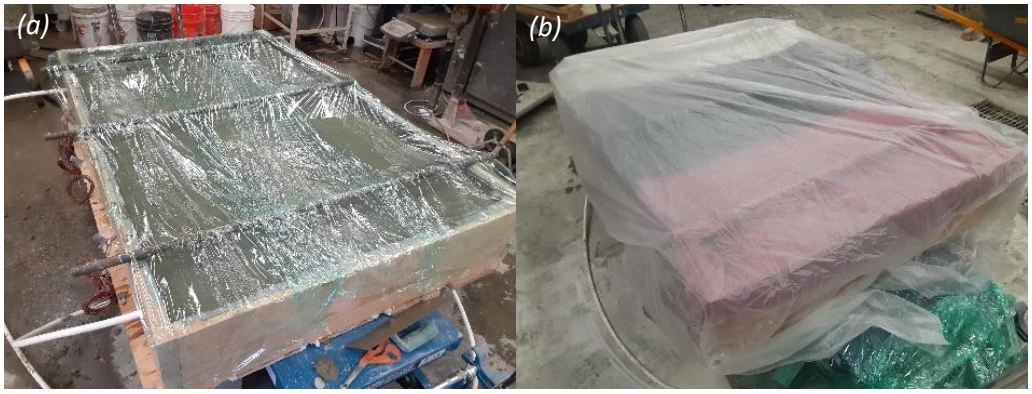

Figure 13. a) Initial 24-hour set and b) 28-day damp towel cure

Bridge Deck Test Preparation

After 28 days, the bridge deck model test preparation began. The steel on top of the forms was removed by stripping the wires at the surface of the concrete. The wood formwork was then removed, taking care not to damage the thermocouples. The wires holding up the top steel reinforcement grid caused some finishing issues in the six locations where wire was used. The rough areas were grinded smooth with a grinder. Figure 14 shows the bridge deck model after the steel and wood formwork were removed.

Figure 14. Cured bridge deck model

After the initial test preparation was completed, the model was moved from the Bulk Materials Lab (Cobleigh 109) to the CHC (Cobleigh 112C) (Figure 15(a)). Hydraulic scissor lift tables were

used to transport the bridge deck once inside Cobleigh Hall (Figure 15(b)). After passing through the SRL into the CHC (Figure 15(c)), the bridge deck model was placed on cinder blocks in its final location (Figure 15(d)).

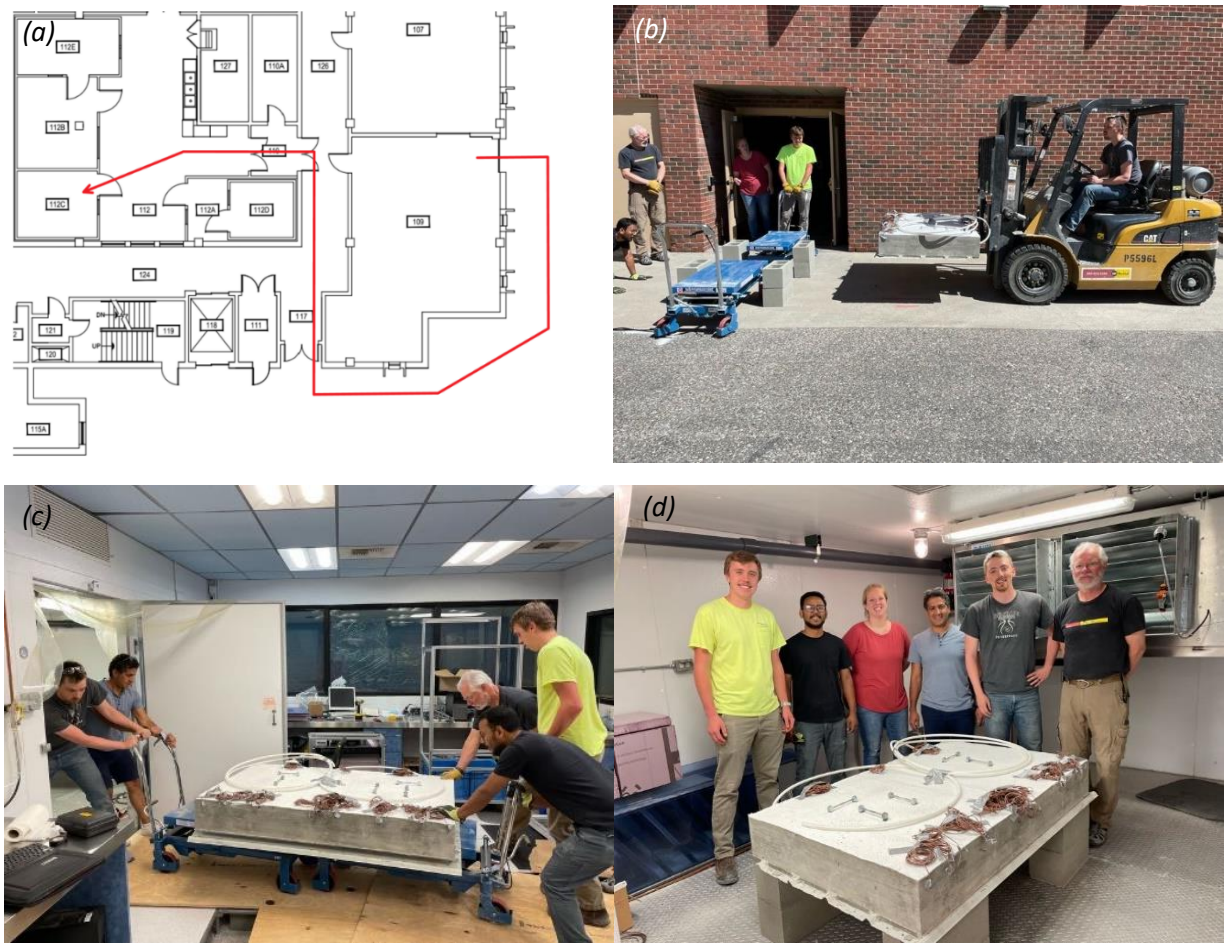

Figure 15. a) Path to CHC, b) transferring bridge deck model to hydraulic scissor lift tables, c) entering the CHC, and d) final bridge deck model position

Once the model was moved to the CHC, the PEX tubing was attached to an inlet valve on one end and allowed to drain into an outlet reservoir on the other. To complete the preparation process, insulation was added to the sides of the model and the exposed PEX tubing.

Figure 16 shows the bridge deck model in the CHC prepared for testing.

Instrumentation

The objective of the physical bridge deck experiments is to further validate the numerical simulation's ability to assess the feasibility of using geothermal energy in Montana to 1) deice concrete bridge decks and 2) mitigate bridge deck cracking. To achieve this, data is needed for the internal and external concrete temperature and the concrete strain. Figure 17(a) and (b) shows the general schematic of the instrumentation and the proposed locations of the thermocouples and strain gauges, respectively. Imbedded Type-T thermocouples (x30) were installed to monitor the internal temperature of the specimen. A thermal camera was used to supplement the thermocouple

data by monitoring the surface temperature of the specimen. GEOKON vibrating wire strain gauges (x5) were used to monitor strain in the bridge deck model.

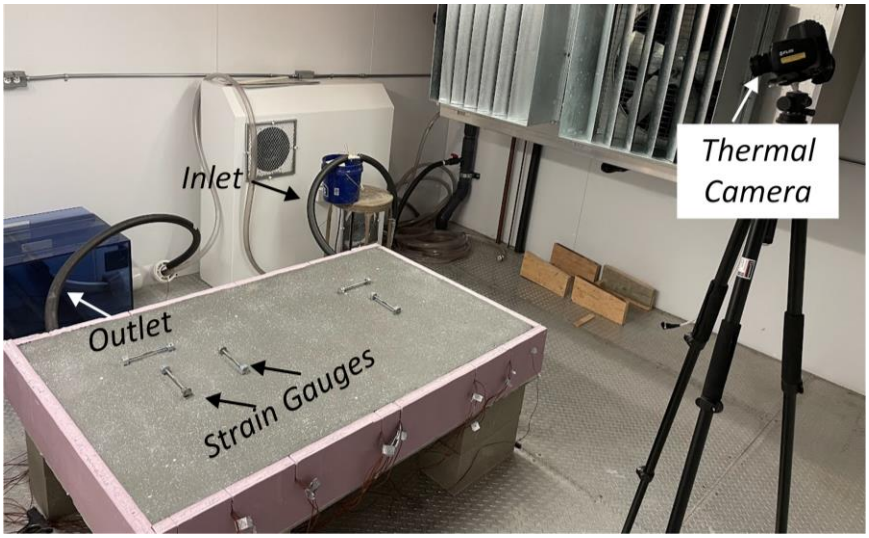

Figure 16. Bridge deck model prepared for testing

Other instrumentation was used to measure the conditions in the CHC. An anemometer was used to measure the wind speed from the CHC fans and a pyranometer was used to measure the solar intensity of the solar simulator. Additional thermocouples were added to measure the ambient temperature and the inlet and outlet fluid temperatures. A McMaster-Carr flow meter was attached near the inlet to measure the flow rate.

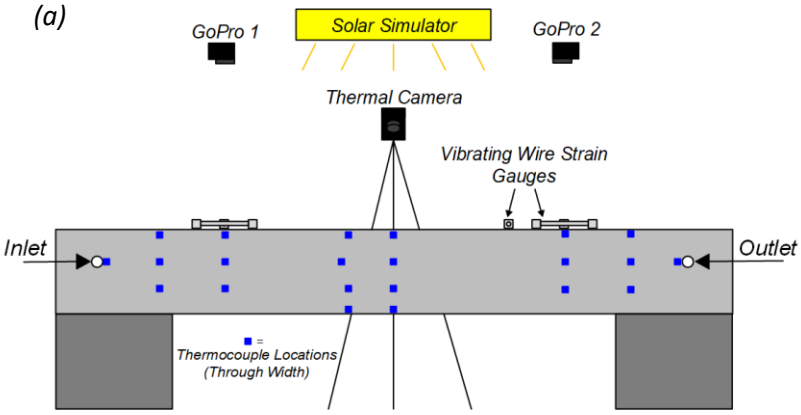

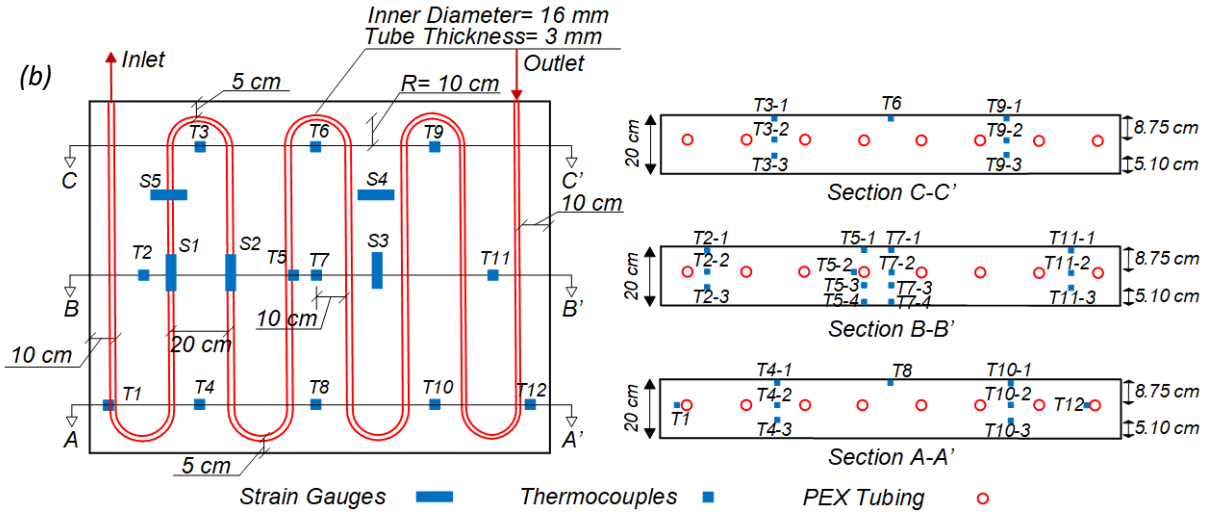

Figure 17. a) Instrumentation schematic and b) proposed locations of thermocouples and strain gauges

Thermocouple Preparation

The thermocouples were prepared using a thermocouple welder. The process includes unwelded thermocouples (Figure 18(a)) being placed in a copper holder, then inserted in the thermocouple welder (Figure 18(b)). The welded thermocouples (Figure 18(c)) were then validated using a mixture of ice and water at approximately 0 °C.

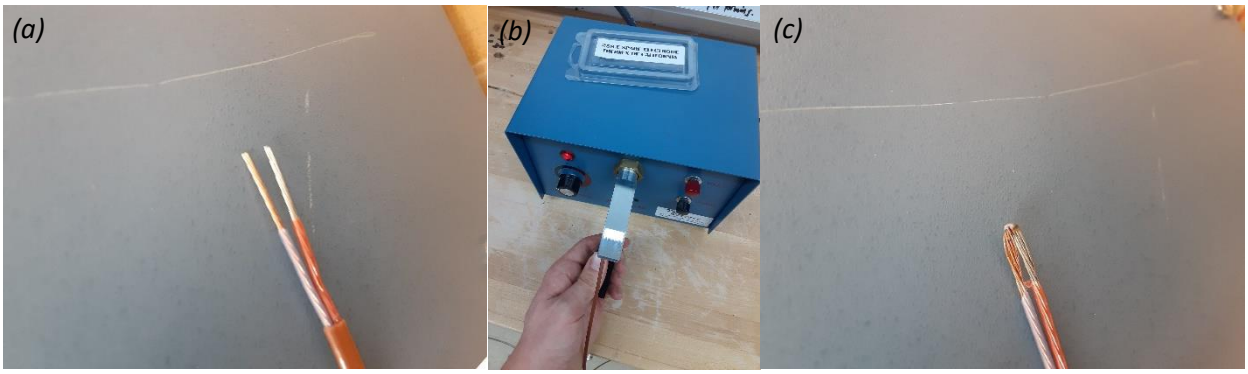

Figure 18. a) Thermocouples before welding, b) thermocouple welder, c) and welded thermocouple

Once validated, the thermocouples were placed using zip ties. Figure 19(a) and (b) show the placed thermocouples. Holes were drilled in the wood formwork for the thermocouples to be fed through.

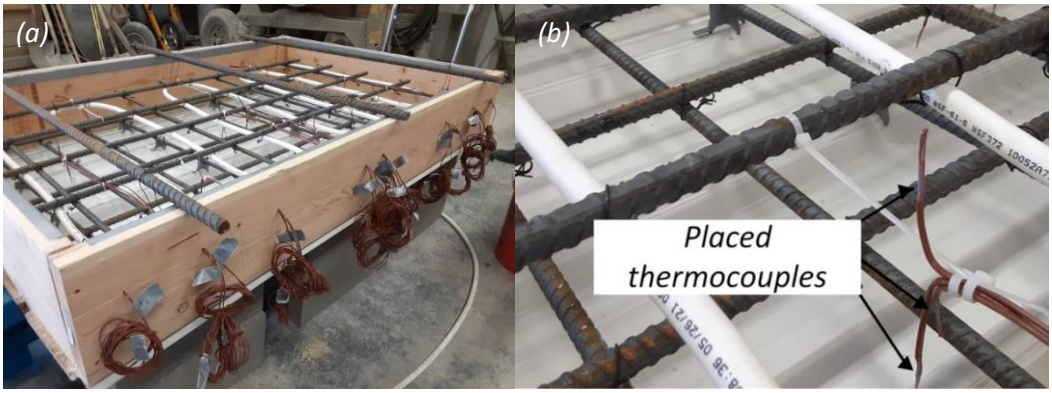

Figure 19. a) Completed form with thermocouples and b) closeup of placed thermocouple

Vibrating Wire Strain Gauge Installation

The GEOKON wire strain gauges were installed by epoxying the mounting blocks into drilled holes in the top surface. Figure 20(a) and (b) shows the strain gauges and mounting blocks before and after placement.

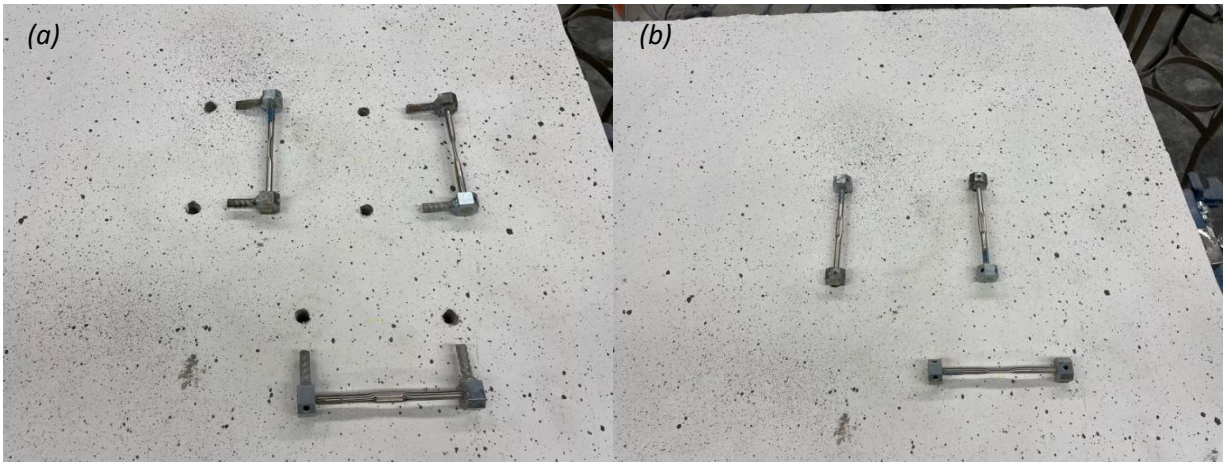

Figure 20. a) Strain gauges with mounting blocks ready for epoxy and b) installed strain gauges

CHAPTER 5: WEATHER SCENARIOS

RWIS stations provide detailed weather information which can be used for winter road and bridge maintenance (Al-Kaisy & Ewan, 2017). The 73 stations in Montana include an air temperature and humidity sensor, wind speed and direction sensor, in-pavement temperature sensor, subsurface temperature sensor, precipitation sensor, and a camera. Figure 21(a) shows the locations of the 73 RWIS stations in Montana. Time histories of the weather data from the 73 RWIS stations were collected from 2015 to 2020. The data indicates that November through February were the coldest months of the year from 2015 to 2020 (Figure 21(c)). To test the feasibility of a ground-source bridge deck deicing system, extreme conditions from these months must be considered. A weather event recorded in Great Falls, MT, in January 2019, was selected for preliminary testing. Figure 21(b) shows the details of the weather event. With temperatures below freezing and high snow accumulation, the Great Falls event represents extreme weather in Montana.

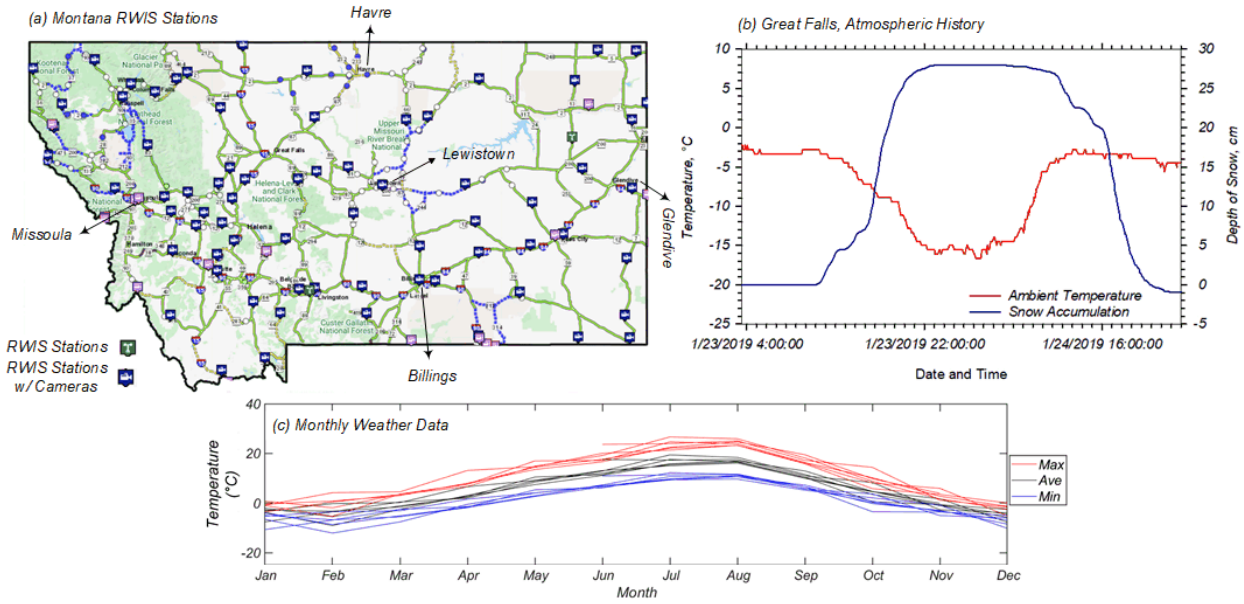

Figure 21. a) Locations of MDT RWIS sites (map source: https://roadreport.mdt.gov/), b) atmospheric history of Great Falls, MT, on January 23-24, 2019, c) and monthly average ambient temperature for 2015-2020

Weather Scenarios

Data from the RWIS stations was used to develop testing scenarios for a geothermal bridge deck deicing system in Montana. The four stages of testing are: synthetic, daily fluctuation, long-term fluctuation, and Montana weather scenarios.

Synthetic

A series of variables were tested with and without the geothermal heat system running in the synthetic test. Figure 22 shows the synthetic testing procedure. The specimen was first tested without the geothermal heat system running. Each phase of the test lasted 12 hours or however long the internal temperatures took to stabilize. First, the model was left to reach equilibrium with the non-cooled room temperature. Then, the ambient temperature was dropped to -10 °C. After 12 hours at -10 °C, the solar simulator was activated. The solar simulator was run at its maximum

intensity of around 488 W/m^2. In the last phase, the ambient temperature was dropped to -20 °C. The entire process was then be repeated while the geothermal heat system was running.

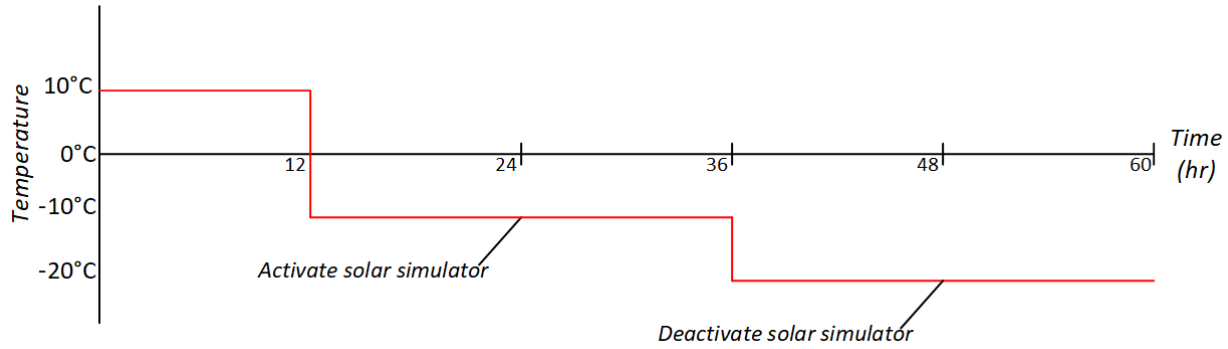

Figure 22. Synthetic testing procedure

Daily Fluctuation

In Montana, large daily temperature fluctuations are experienced during March and April. The second stage of testing simulated these fluctuations. Figure 23 illustrates the daily fluctuation testing procedure. The ambient temperature started at the average daily maximum temperature for March and April. After 3 hours at the maximum, the temperature was gradually dropped over a period of 6 hours to the average daily minimum temperature for March and April. Once the temperature reached the minimum, it remained constant for a period of 6 hours. After that, it was gradually returned to the maximum temperature over a period of 6 hours. This temperature remained constant at the maximum for 3 hours. The 24-hour cycle was repeated to simulate consecutive days.

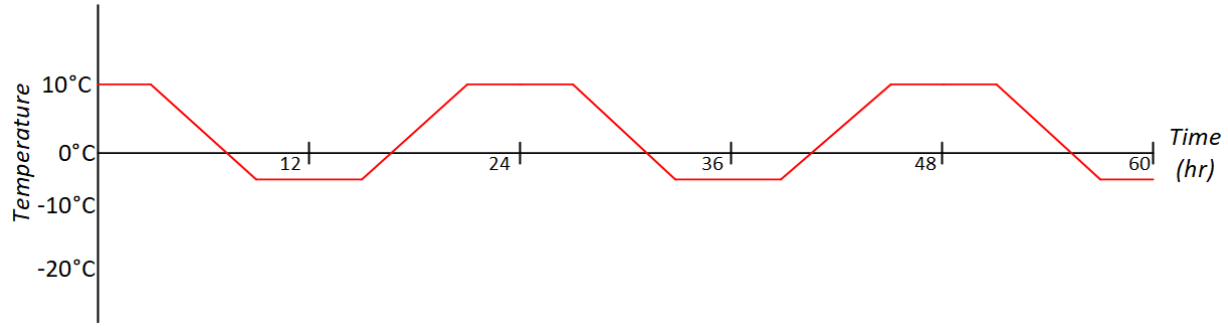

Figure 23. Daily fluctuation testing procedure

Long-Term Fluctuation

Montana experiences a significant difference between its annual maximum and minimum temperatures. The third stage of testing simulated these large temperature fluctuations. Figure 24 illustrates the long-term fluctuation testing procedure. The ambient temperature began at the CHC's maximum ambient temperature of 10 °C. After 24 hours at 10 °C, the ambient temperature was dropped to Montana's average annual minimum temperature. The temperature remained at the minimum for 24 hours, after which it rose back to 10 °C.

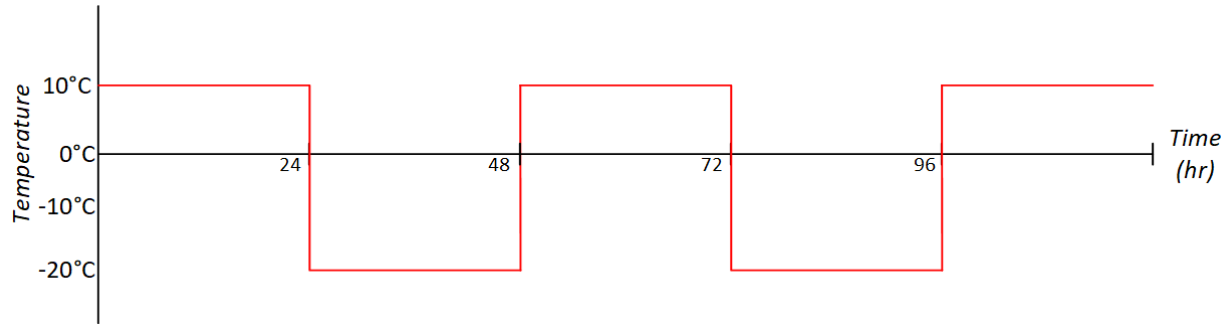

Figure 24. Long-term fluctuation testing procedure

Weather Scenarios based on Montana Weather

First Scenario- Severe Winter Event- Great Falls, January 23-24, 2019

The first Montana weather scenario that was replicated is a severe winter event that occurred in Great Falls in January 2019. Figure 25 illustrates the time histories of the ambient temperature and cumulative snowfall on January 23-24, 2019. The data indicates that 28 cm of snow accumulated over the course of 10 hours on January 23, 2021. The ambient temperature during the snowfall varied between -2 °C to -17 °C.

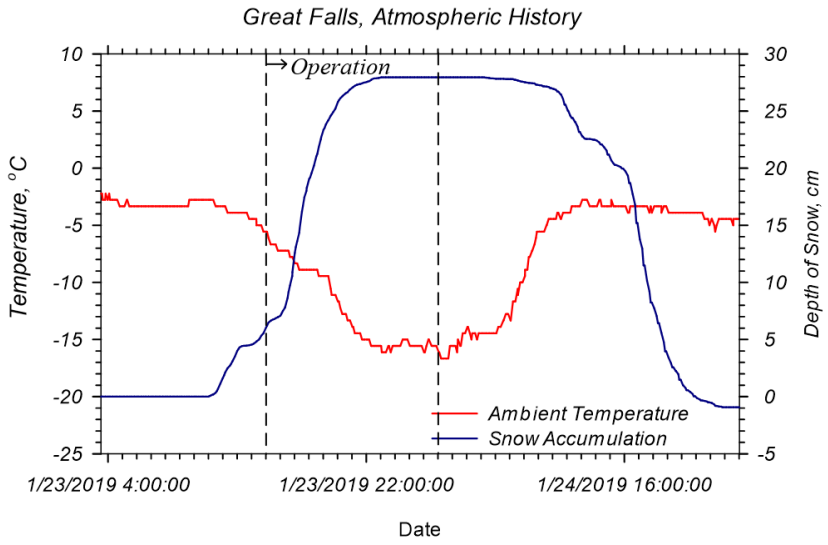

Figure 25. Atmospheric history of Great Falls, MT, on January 23-24, 2019

Second Scenario- Moderate Winter Event- Missoula, Lookout Pass, February 11-13, 2019

The second Montana weather that was replicated is a moderate winter event that occurred in Missoula in February 2019. Figure 26 shows the ambient temperature and cumulative snowfall recorded in Missoula, Montana during the event. The snowfall began on February 11, 2019, around 22:00 and continued until February 13, 2019, 6:00. The recorded data indicated that the snow accumulated at a higher rate between the hours of 7:00 and 17:00 on February 12, 2019. The ambient temperature varied between -2 °C and -9 °C during the storm.

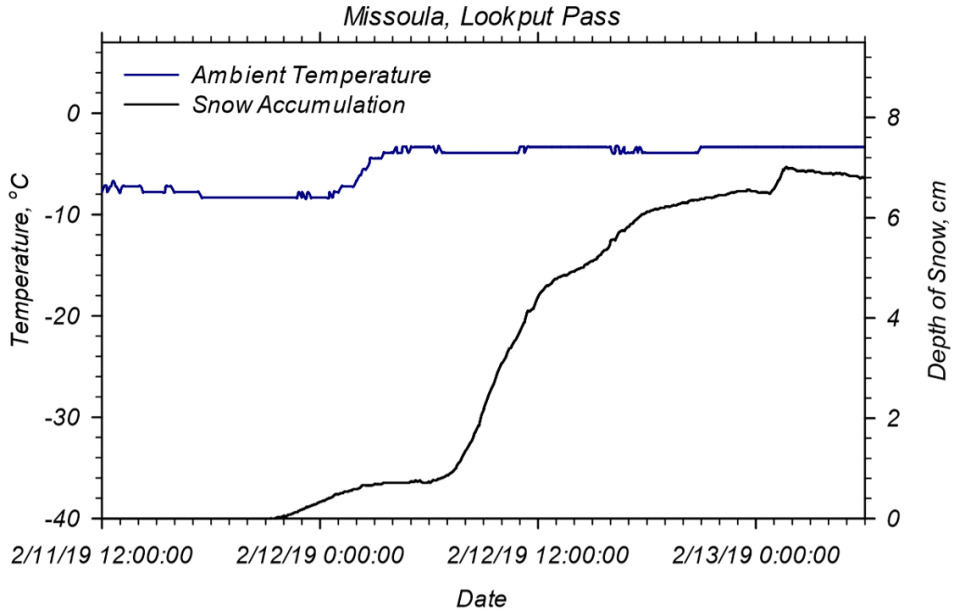

Figure 26. Atmospheric history of Lookout Pass, Missoula, MT, on February 11-13, 2019

CHAPTER 6: PRELIMINARY RESULTS

Detailed analyses of the results and a comparison with the numerical model will be provided in the future for all testing scenarios. In this task report, the preliminary results for the synthetic scenario are provided for thermocouples at each depth in between the heat exchanger tubes. During trial tests, representative thermocouples at each depth were identified to assess overall results due to their response to different stimuli. Figure 27 shows the representative thermocouples and their depth, y, from the top of the bridge deck. T7-4 was chosen to represent the temperature of the bottom of the concrete because it is the only thermocouple at the bottom of the concrete and in between the heat exchanger tubes. For the top of the concrete, T8 was chosen due to its immediate response to solar simulation. T11-2 was chosen for the depth in line with the heat exchanger tubes due to its immediate response to turning on the geothermal system. For the depth in between the heat exchanger tubes and the bottom of the concrete, T10-3 was chosen.

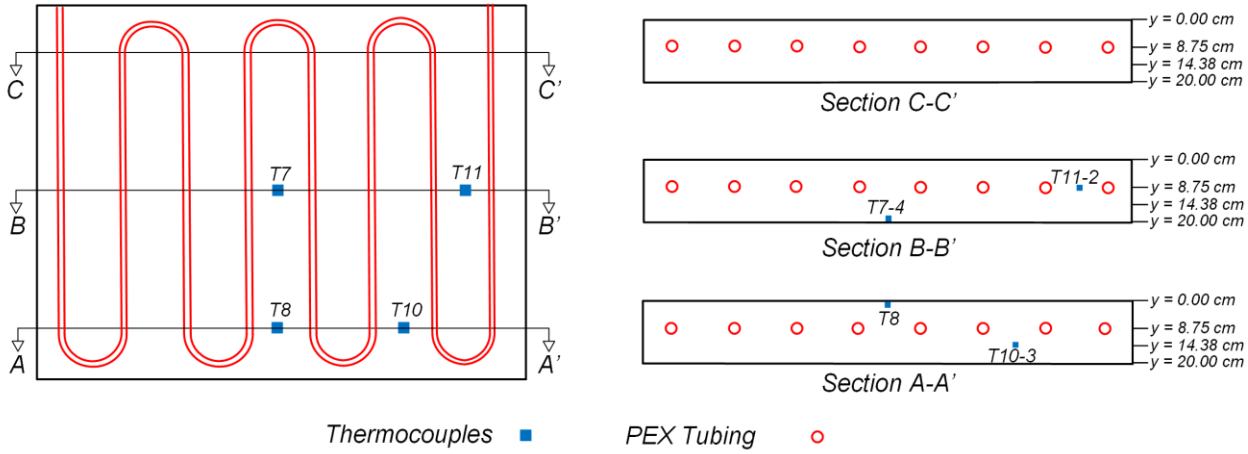

Figure 27. Representative thermocouples at each depth

Synthetic Results

The purpose of the synthetic test was to compare the temperature at which the bridge deck stabilized under different weather conditions with and without the geothermal system running. Both tests were exposed to the same weather conditions as described in Figure 22. An average wind speed of 4.0 mph over the deck from the CHC fans was measured with the anemometer for both tests. A solar intensity of around 488 W/m^2 was measured with the pyranometer for all solar simulation scenarios in the tests. This intensity was used because it is the maximum intensity of the solar simulator and is closest to the maximum solar intensity in Montana.

Without Geothermal System Running

The testing program without the geothermal system running differed slightly from the program described in Figure 22. The CHC has routine defrost cycles which occur every 12 hours to maintain the state of the lab, which results in temperature spikes every 12 hours. Figure 28(a) shows the measured weather conditions throughout the test without the geothermal system running. The test consists of four stages: in Stage 1, the ambient temperature is -10 °C without solar simulation; in Stage 2, the ambient temperature remains at -10 °C with a solar intensity of about 488 W/m^2; in Stage 3, the ambient temperature drops to -20 °C while the solar intensity remains constant; in Stage 4, the ambient temperature stays at -20 °C without solar simulation. Figure 28(b) shows the temperature at different depths of the bridge deck. In Stages 1 and 4 without solar simulation, the

concrete temperature for all depths stabilized at a temperature around the ambient temperature. In stages 2 and 3 with solar simulation, the concrete temperature at all depths stabilized at a temperature above the ambient temperature. The temperature of T8 was affected the most by the solar simulation with stabilized temperatures of 2.9 °C and -7.0 °C for Stages 2 and 3, respectively. The effect of the solar simulation decreased as the depth increased with the temperature of T7-4 being least affected with stabilized temperatures of -4.6 °C and -14.4 °C for Stages 2 and 3, respectively.

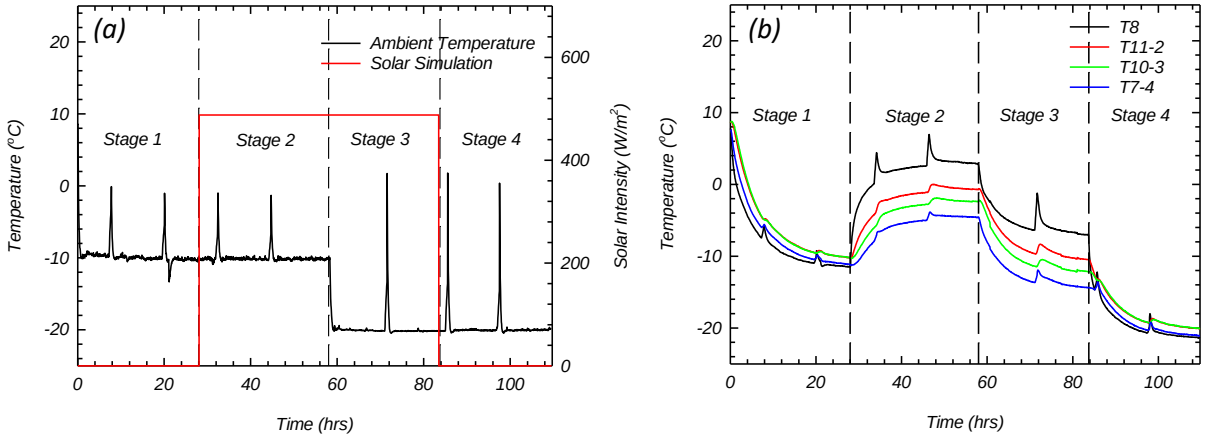

Figure 28. a) Ambient temperature and solar intensity and b) concrete temperature at different depths for test without geothermal system running

Table 2 summarizes the stabilized temperatures at all depths and weather conditions for the test without the geothermal heating system running. Stages 1 and 4 both have a maximum temperature gradient of 1.2 °C between T8 and T11-2/T10-3. This small temperature gradient is due to the top and bottom of the concrete being exposed to the ambient temperature and wind while the middle of the concrete is not. Stage 2 and 3 have maximum temperature gradients between T8 and T7-4 of 7.4 °C and 7.5 °C, respectively. These larger temperature gradients are because the solar simulator effect is greatest at the top surface of the concrete and lowest at the bottom of the concrete.

Table 2. Stabilized temperatures without geothermal system running

Thermocouple	*Stage 1: Stabilized Temp. @ -10 °C w/o solar (°C)*	*Stage 2: Stabilized Temp. @ -10 °C w/ solar (°C)*	*Stage 3: Stabilized Temp. @ -20 °C w/ solar (°C)*	*Stage 4: Stabilized Temp. @ -20 °C w/o solar (°C)*
T8	-11.5	2.9	-7.0	-21.4
T11-2	-10.3	-0.7	-10.5	-20.2
T10-3	-10.3	-2.4	-12.2	-20.2
T7-4	-11.3	-4.6	-14.4	-21.1

With Geothermal System Running

The same testing program was used for the test with the geothermal system running with defrost cycles occurring every 12 hours. In the first 20 hours, two additional defrost cycles occurred. Figure 29(a) shows the measured weather conditions throughout the test with the geothermal system running. The stages in this test followed the same program as for the test without the geothermal system running. Figure 29(b) shows the concrete temperature at different depths for the testing scenario. The concrete temperature at all depths and during all stages stabilized at a temperature above the ambient temperature. During Stage 1 and 4, the maximum stabilized

temperatures were located at T11-2 with stabilized temperatures of -1.8 °C and -8.2 °C. T11-2 measured the maximum stabilized temperatures because it is the closest to the heat exchanger tubes. T10-2 measured the second highest temperatures of -2.2 °C and -8.9 °C for Stages 1 and 4, respectively, because it is the next closest to the heat exchanger tubes. T8 measured the third highest temperatures of -5.3 °C and -12.6 °C for Stages 1 and 4, respectively. These temperatures are much lower than the previous depths because the top is exposed to the ambient temperature and wind. T7-4 measured the lowest temperature of -5.6 °C and -13.3 °C for Stages 1 and 4, respectively, because it is the farthest from the heat exchanger tubes and it is exposed to the ambient temperature and wind. During Stages 2 and 3, the maximum stabilized temperatures were located at T8 with stabilized temperatures of 5.4 °C and -1.3 °C, respectively. The top of the concrete measured the maximum stabilized temperatures because the effect of the solar simulator overpowered the effect of the heat exchanger tubes. As with the test without the geothermal system running, the effect of the solar simulation decreased as the depth increased with the lowest stabilized temperatures for Stages 2 and 3 measured at T7-4 (-2.4 °C and -9.3 °C, respectively).

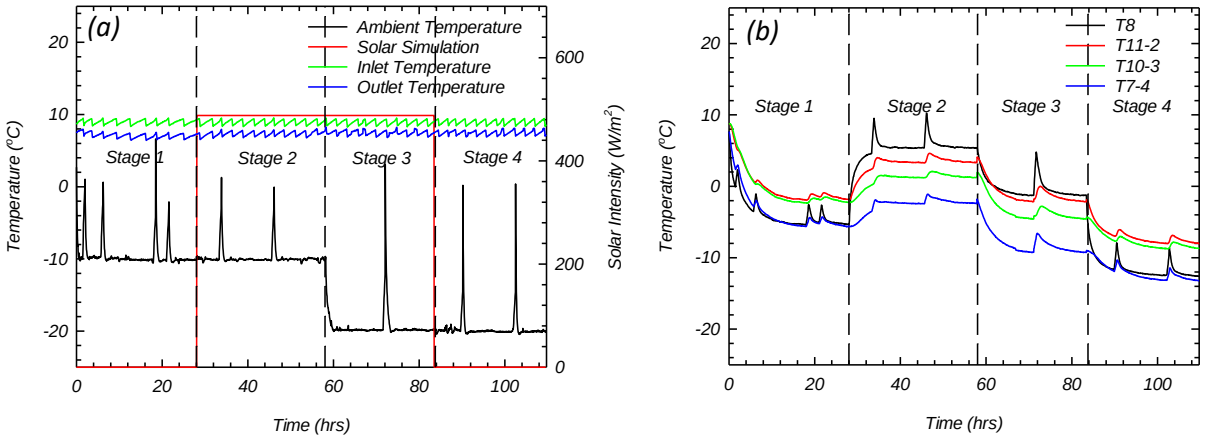

Figure 29. a) Ambient temperature and solar intensity and b) concrete temperature at different depths for test with geothermal system running

Table 3 summarizes the stabilized temperatures at all depths and weather conditions for the test with the geothermal system running. Stages 1 and 4 have maximum temperature gradients of 3.8 °C and 5.1 °C, respectively between T11-2 and T7-4. These temperature gradients are due to T11-2 being closest to the heat exchanger tube, and T7-4 being farthest from it. Stages 2 and 3 have maximum temperature gradients of 7.8 °C and 8.0 °C, respectively between the T8 and T7-4. These temperature gradients are similar to the gradients measured during the test without the geothermal system running because the effect of the solar simulator overpowers the effect of the heat exchanger tubes.

Table 3. Stabilized temperatures with geothermal system running

Thermocouple Location	*Stage 1: Stabilized Temp. @ -10 °C w/o solar (°C)*	*Stage 2: Stabilized Temp. @ -10 °C w/ solar (°C)*	*Stage 3: Stabilized Temp. @ -20 °C w/ solar (°C)*	*Stage 4: Stabilized Temp. @ -20 °C w/o solar (°C)*
T8	-5.3	5.4	-1.3	-12.6
T11-2	-1.8	3.4	-2.2	-8.2
T10-3	-2.2	1.2	-4.6	-8.9
T7-4	-5.6	-2.4	-9.3	-13.3

Conclusions

A physical geothermally heated bridge deck model was tested under synthetic conditions to provide further validation of a numerical model of a geothermal bridge deck deicing system. Under synthetic conditions, the temperature at which different depths of the concrete stabilized was found for the bridge deck with and without the geothermal system running. Results show that the stabilized temperatures at all depths of the concrete and during all stages were greater when the geothermal system was running. The maximum difference between the top surface temperature of the concrete with and without the geothermal system running occurred when the ambient temperature was -20 °C and there was no solar simulation (Stage 4). For this stage, the stabilized top surface temperatures of the test without and with the geothermal system running are -21.4 °C and -12.6 °C, respectively. Figure 30 shows the top surface temperature for both tests. The temperature gradients for the test with the geothermal system running were greater than when the geothermal system was not running during stages without solar simulation. During stages with solar simulation, the temperature gradients were similar between both tests.

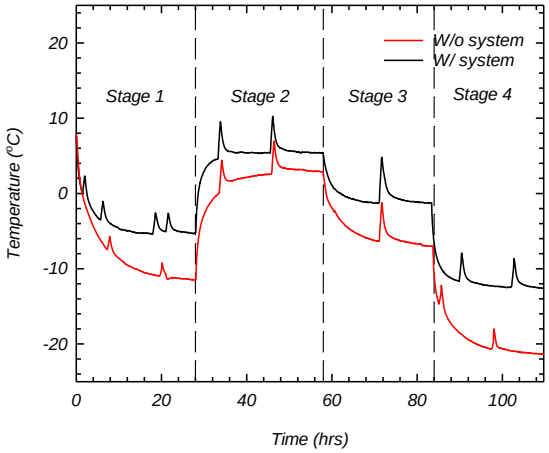

Figure 30. Top surface concrete temperatures of tests with and without geothermal system running

Preliminary results show that the use of geothermal energy to deice bridges in Montana is better suited for certain weather conditions than others. Once the remaining testing programs are completed in the CHC, the numerical model will be validated and ready to evaluate how various weather conditions affect the feasibility of using geothermal energy to deice bridges in Montana.

REFERENCES

Al-Kaisy, A., & Ewan, L. (2017). Prioritization scheme for proposed road weather information system sites: Montana case study. *Frontiers in built environment, 3*, 45.

Baboian, R. (1992). Synergistic effects of acid deposition and road salts on corrosion. In *Corrosion forms and control for infrastructure* (pp. 17-29). ASTM International.

Bowers Jr, G. A. (2016). Ground-source bridge deck deicing and integrated shallow geothermal energy harvesting systems [*Doctoral dissertation, Virginia Tech*].

Fischel, M. (2001). Evaluation of selected deicers based on a review of the literature. *CDOT-DTD-R-2001-15*, 160. (*Colorado Department of Transportation*).

Granata, R., & Hartt, W. H. (2009). Integrity of infrastructure materials and structures. *U.S.D.o.T. FHWA, ed., FHWA, U.*S. Department of Transportation, United States, 90p.

Kelting, D. L., & Laxon, C. L. (2010). Review of effects and costs of road de-icing with recommendations for winter road management in the Adirondack Park. *Adirondack Watershed Institute.*

Nagy, B., & Szagri, D. (2018). Thermophysical behaviour of reinforced concretes. In *Proc., 6th Int. Conf. Contemporary Achievements in Civil Engineer* (pp. 243-253).

Pourakbar, M., Plymesser, K., Khosravi M., Gunyol, P., Phillips, A., SEN, T., & Perkins, S. (2021). Task Report No 2: A feasibility of road culvert/bridge deck deicing using geothermal energy. Available online (https://www.mdt.mt.gov/other/webdata/external/research/docs/research_proj/DEICING-GEOTHERMAL/Task-2-Report.pdf)

Shi, X., Du, S., & Fay, L. (2018). Environmental Risks of Snow and Ice Control Materials. *Sustainable Winter Road Operations,* 180-210.

Virmani, Y., Clear, K., Pasko Jr, T., Jones, W., & Jones, D. (1983). Time-to-corrosion of reinforcing steel in concrete slabs. Volume 5: Calcium nitrite admixture or epoxy-coated reinforcing bars as corrosion protection systems. *STIN, 84*, 32578.

Virmani, Y. P., Jones, W. R., & Jones, D. H. (1984). pH at Corrosion Sites. *Public Roads, 48*(3), 96-102.

White, D., Sritharan, S., Suleiman, M. T., & Chetlur, S. (2005). Identification of the best practices for design, construction, and repair of bridge approaches. *Final Report*, Iowa DOT TR-481, CTRE Report 02-118.

Yunovich, M., Thompson, N., & Virmani, Y. P. (2003). Life cycle cost analysis for reinforced concrete bridge decks. *CORROSION 2003, San Diego, California*, 03309.

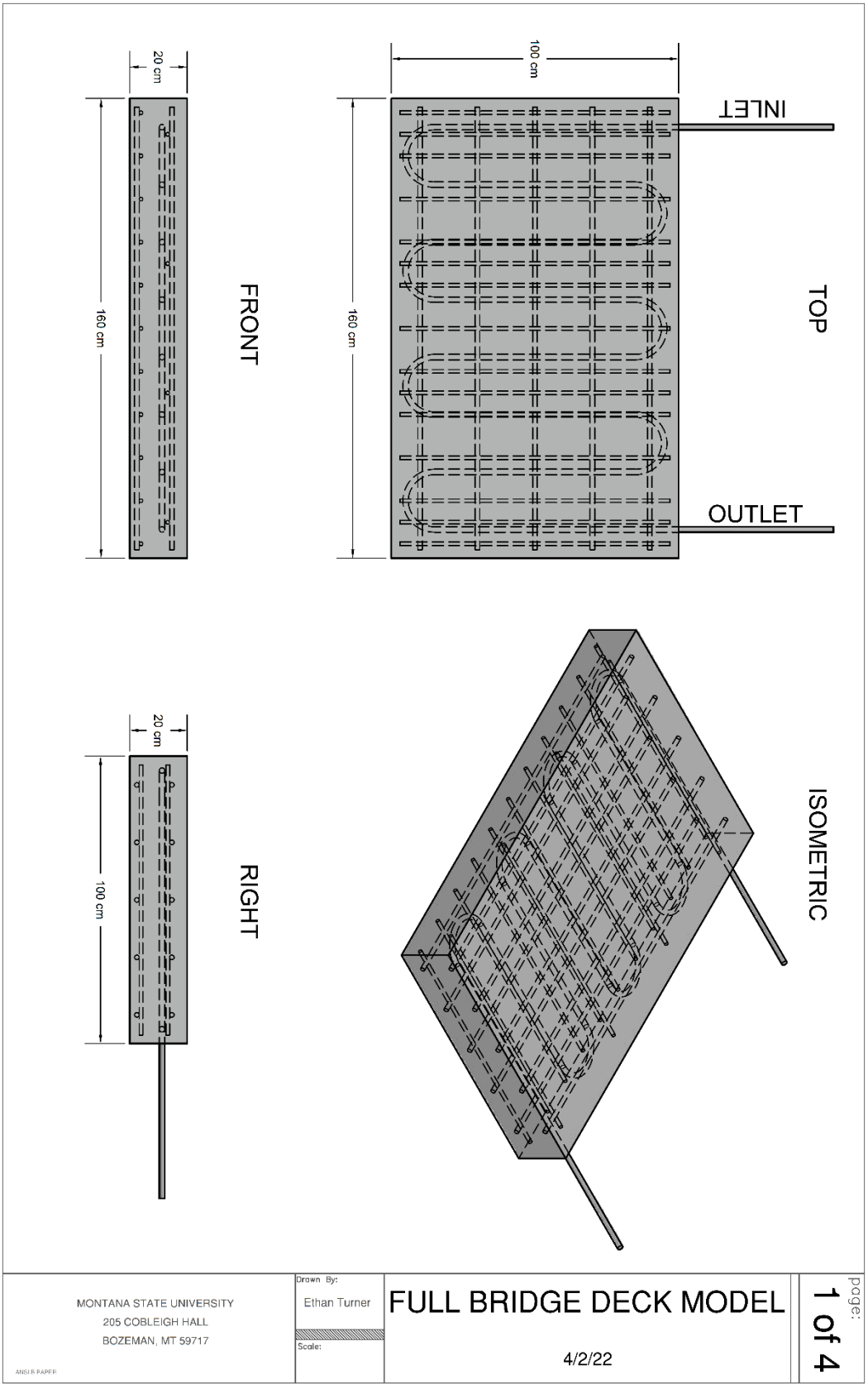
20 cm
160 cm
FRONT
100 cm
160 cm
INLET
TOP
OUTLET
20 cm
100 cm
RIGHT
ISOMETRIC
MONTANA STATE UNIVERSITY
205 COBLEIGH HALL
BOZEMAN, MT 59717
ANSI B PAPER
Drawn By:
Ethan Turner
Scale:
FULL BRIDGE DECK MODEL
4/2/22
page:
1 of 4

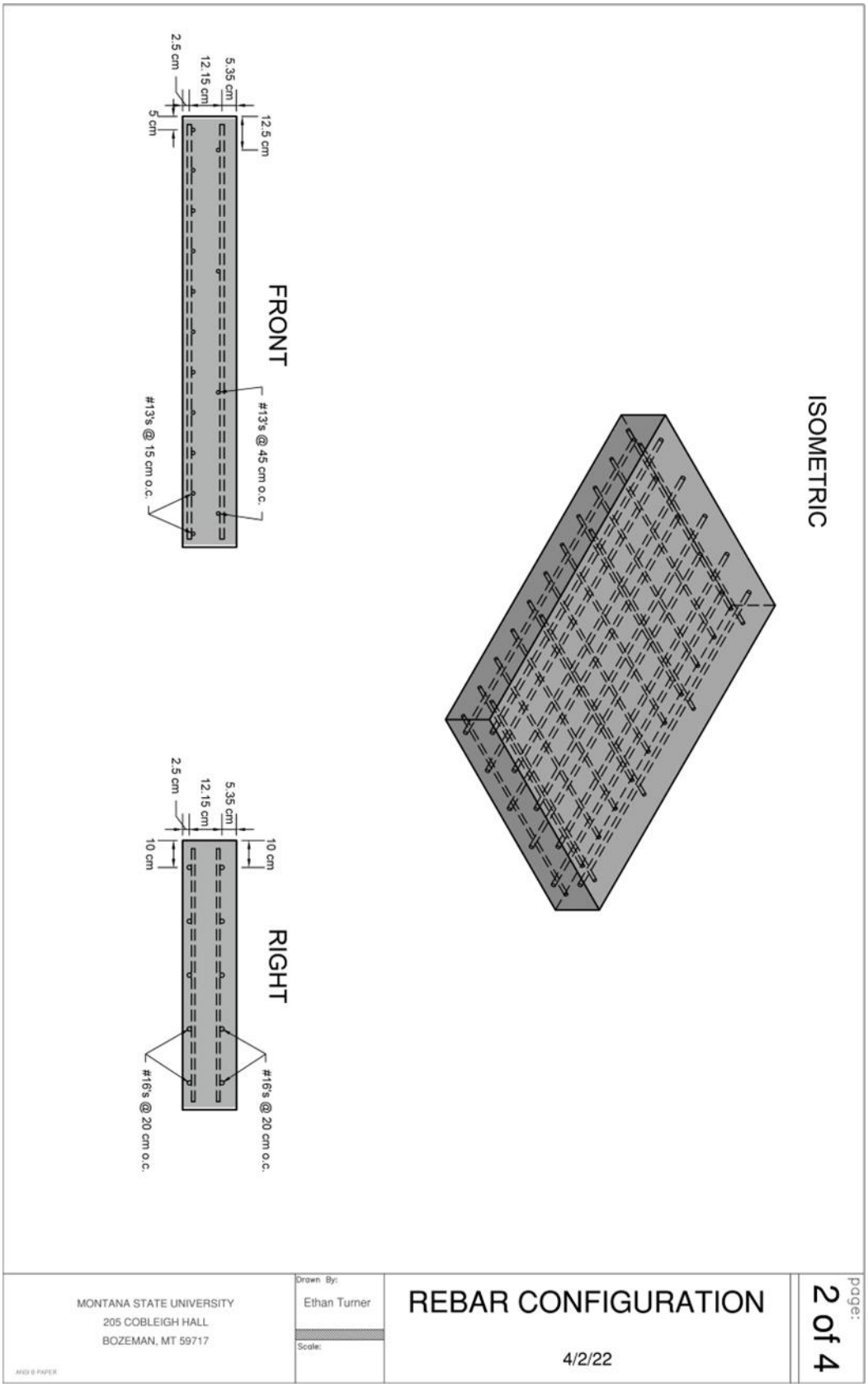
FRONT
2.5 cm
5.35 cm
12.15 cm
5 cm
12.5 cm
#13's @ 45 cm o.c.
#13's @ 15 cm o.c.
ISOMETRIC
RIGHT
2.5 cm
5.35 cm
12.15 cm
10 cm
10 cm
#16's @ 20 cm o.c.
#16's @ 20 cm o.c.
MONTANA STATE UNIVERSITY
205 COBLEIGH HALL
BOZEMAN, MT 59717
Drawn By:
Ethan Turner
Scale:
REBAR CONFIGURATION
4/2/22
page:
2 of 4

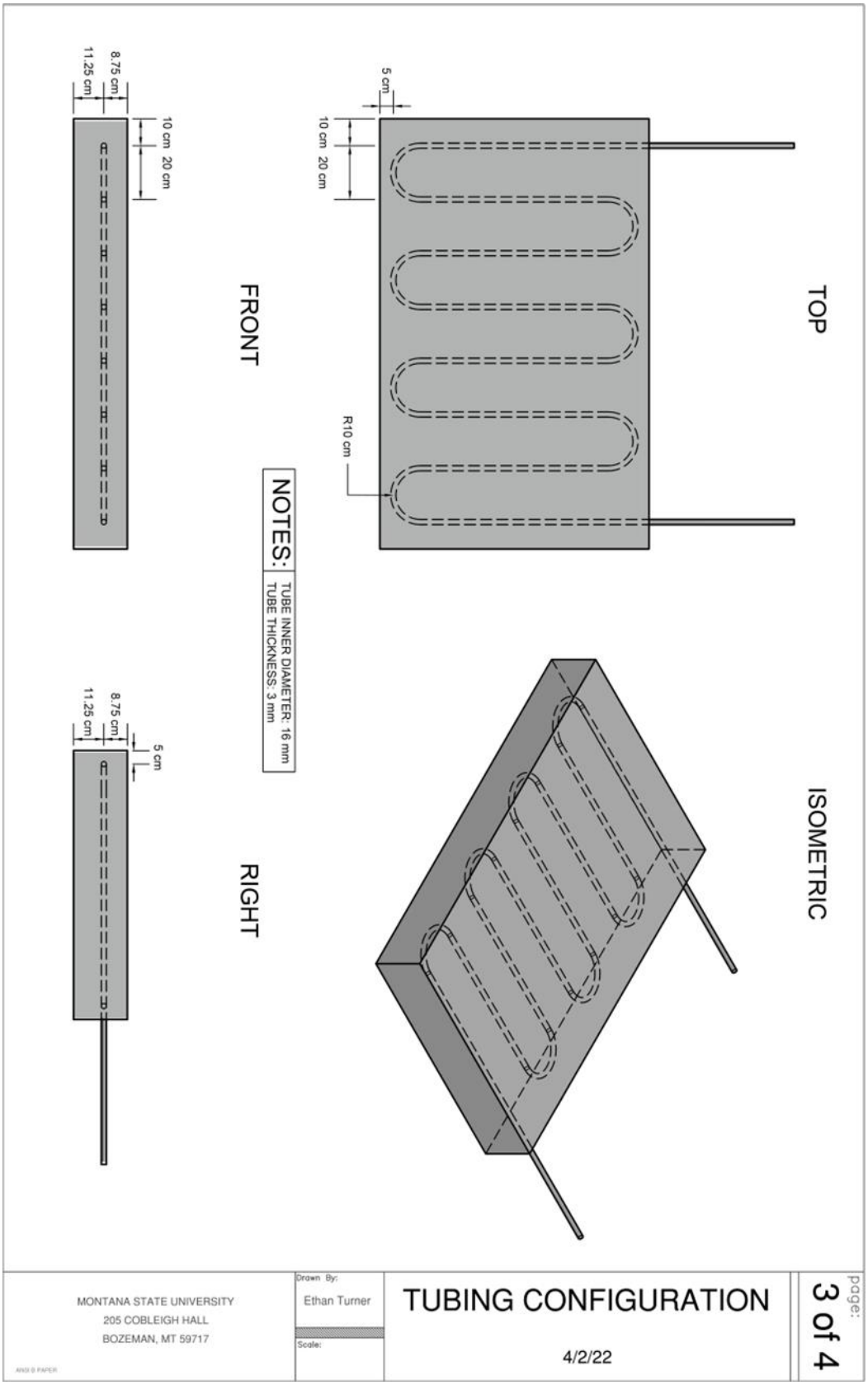
TOP
5 cm
10 cm 20 cm
R10 cm
FRONT
11.25 cm
8.75 cm
10 cm 20 cm
NOTES:
TUBE INNER DIAMETER: 16 mm
TUBE THICKNESS: 3 mm
ISOMETRIC
RIGHT
11.25 cm
8.75 cm
5 cm
MONTANA STATE UNIVERSITY
205 COBLEIGH HALL
BOZEMAN, MT 59717
Drawn By:
Ethan Turner
Scale:
TUBING CONFIGURATION
4/2/22
page:
3 of 4

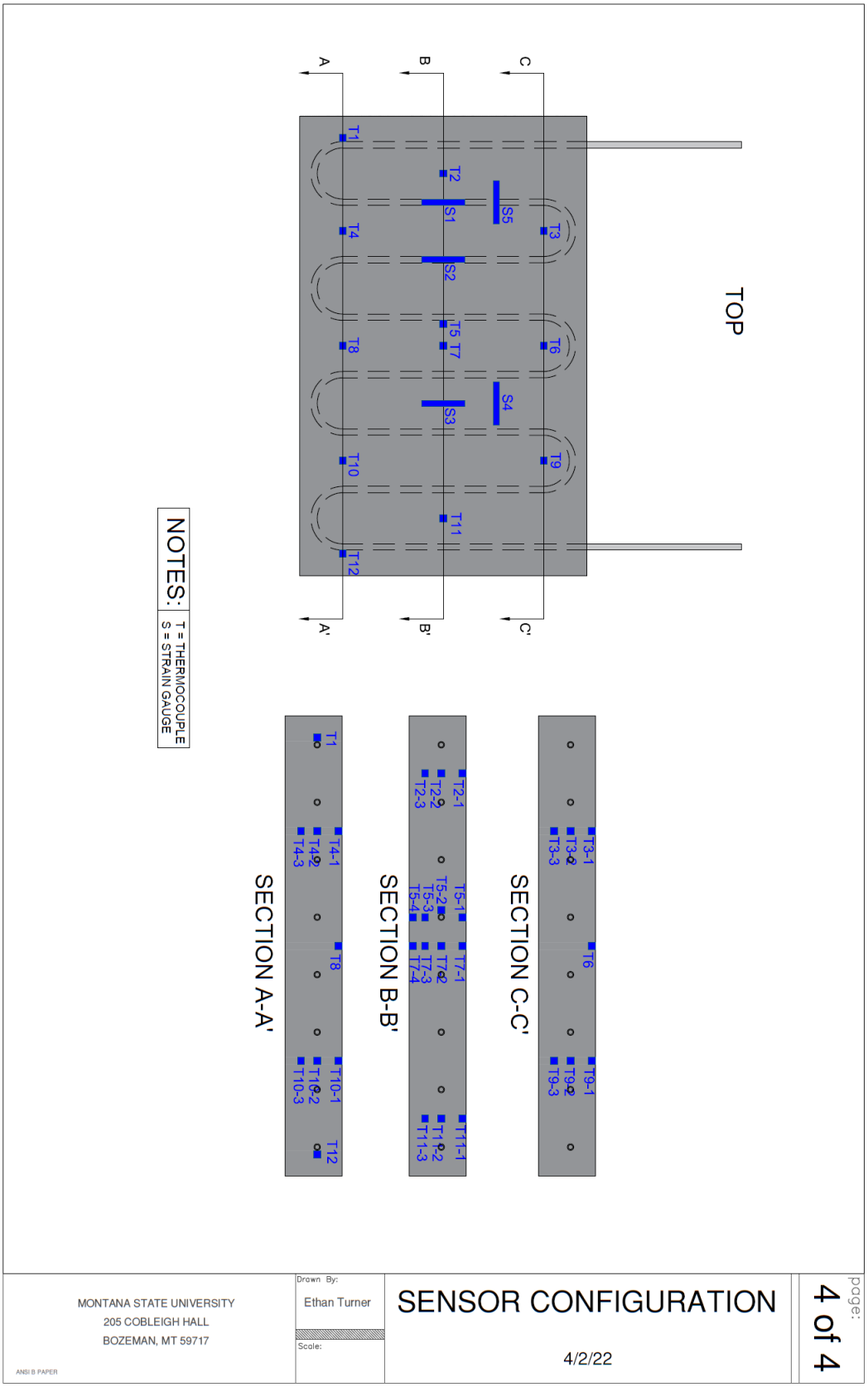
TOP
A
B
C
A'
B'
C'
T1
T2
T3
T4
T5
T6
T7
T8
T9
T10
T11
T12
S1
S2
S3
S4
S5
NOTES:
T = THERMOCOUPLE
S = STRAIN GAUGE
SECTION A-A'
SECTION B-B'
SECTION C-C'
T1
T4-1
T4-2
T4-3
T8
T10-1
T10-2
T10-3
T12
T2-1
T2-2
T2-3
T5-1
T5-2
T5-3
T5-4
T7-1
T7-2
T7-3
T7-4
T11-1
T11-2
T11-3
T3-1
T3-2
T3-3
T6
T9-1
T9-2
T9-3
MONTANA STATE UNIVERSITY
205 COBLEIGH HALL
BOZEMAN, MT 59717
ANSI B PAPER
Drawn By:
Ethan Turner
Scale:
SENSOR CONFIGURATION
4/2/22
page:
4 of 4